

C9orf72 suppresses systemic and neural inflammation induced by gut bacteria

<https://doi.org/10.1038/s41586-020-2288-7>

Received: 17 May 2019

Accepted: 9 April 2020

Published online: 13 May 2020

 Check for updates

Aaron Burberry^{1,2}, Michael F. Wells^{1,2}, Francesco Limone^{1,2,3}, Alexander Couto^{1,2}, Kevin S. Smith^{1,2}, James Keaney⁴, Gaëlle Gillet⁴, Nick van Gastel^{1,5}, Jin-Yuan Wang^{1,2}, Olli Pietilainen^{1,2}, Menglu Qian^{1,2,6}, Pierce Eggan^{1,2}, Christopher Cantrell^{1,2}, Joanie Mok^{1,2}, Irena Kadju⁴, David T. Scadden^{1,5} & Kevin Eggan^{1,2,6}✉

A hexanucleotide-repeat expansion in *C9ORF72* is the most common genetic variant that contributes to amyotrophic lateral sclerosis and frontotemporal dementia^{1,2}. The *C9ORF72* mutation acts through gain- and loss-of-function mechanisms to induce pathways that are implicated in neural degeneration^{3–9}. The expansion is transcribed into a long repetitive RNA, which negatively sequesters RNA-binding proteins⁵ before its non-canonical translation into neural-toxic dipeptide proteins^{3,4}. The failure of RNA polymerase to read through the mutation also reduces the abundance of the endogenous *C9ORF72* gene product, which functions in endolysosomal pathways and suppresses systemic and neural inflammation^{6–9}. Notably, the effects of the repeat expansion act with incomplete penetrance in families with a high prevalence of amyotrophic lateral sclerosis or frontotemporal dementia, indicating that either genetic or environmental factors modify the risk of disease for each individual. Identifying disease modifiers is of considerable translational interest, as it could suggest strategies to diminish the risk of developing amyotrophic lateral sclerosis or frontotemporal dementia, or to slow progression. Here we report that an environment with reduced abundance of immune-stimulating bacteria^{10,11} protects *C9orf72*-mutant mice from premature mortality and significantly ameliorates their underlying systemic inflammation and autoimmunity. Consistent with *C9orf72* functioning to prevent microbiota from inducing a pathological inflammatory response, we found that reducing the microbial burden in mutant mice with broad spectrum antibiotics—as well as transplanting gut microflora from a protective environment—attenuated inflammatory phenotypes, even after their onset. Our studies provide further evidence that the microbial composition of our gut has an important role in brain health and can interact in surprising ways with well-known genetic risk factors for disorders of the nervous system.

To understand the consequences of the long-term reduction in *C9ORF72* activity found in patients with amyotrophic lateral sclerosis (ALS) or frontotemporal dementia (FTD) who carry the repeat expansion, mice that contain loss-of-function (LOF) mutations in the orthologous gene (*C9orf72*) have previously been studied^{6,7,12,13}. It was previously reported⁷, and later corroborated, that reduced *C9orf72* function led to age-dependent inflammation, characterized by cytokine storm^{7,14}, neutrophilia^{6,7,14}, pseudothrombocytopenia⁷, autoimmunity^{7,14}, splenomegaly^{6,7,13,14} and neuroinflammation^{6,7}. Informed by these observations and validating their importance, it was subsequently found that patients with ALS or FTD who had mutations in *C9ORF72* were significantly more likely to have been diagnosed with autoimmune disease before their neurological diagnosis^{15,16}.

However, the long-term survival of *C9orf72* LOF mutant mice varied markedly between reports, despite many groups studying the same allele on a similar genetic background. In some studies, it was found^{7,12} that the loss of one (+/−) or both (−/−) alleles of *C9orf72* increased the risk of premature mortality, whereas others¹³ noted a reduced survival of *C9orf72*^{−/−} but not *C9orf72*^{+/−} mice—and another group⁶ reported no survival differences between control and mutant mice (Extended Data Fig. 1). These findings suggested that the environment in which the mice were reared might be an important modifier of survival when *C9orf72* levels are reduced. To test this hypothesis, we aseptically re-derived *C9orf72*-mutant mice into a new facility at the Broad Institute (hereafter referred to as *C9orf72*(Broad) mice) while continuing our colony at the Harvard Biological Research Infrastructure (BRI)

¹Harvard Stem Cell Institute, Department of Stem Cell and Regenerative Biology, Harvard University, Cambridge, MA, USA. ²Stanley Center for Psychiatric Research, Broad Institute of MIT and Harvard, Cambridge, MA, USA. ³Hubrecht Institute for Developmental Biology and Stem Cell Research, Royal Netherlands Academy of Arts and Sciences, Utrecht, The Netherlands.

⁴Neuroscience Therapeutic Area, New Medicines, UCB Biopharma SPRL, Braine-l'Alleud, Belgium. ⁵Center for Regenerative Medicine, Massachusetts General Hospital, Boston, MA, USA.

⁶Department of Molecular and Cellular Biology, Harvard University, Cambridge, MA, USA. ✉e-mail: Eggan@mcb.harvard.edu

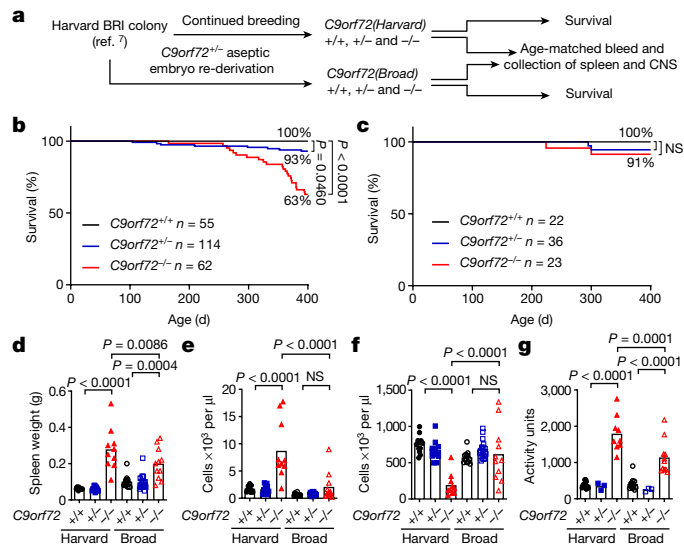


Fig. 1 | Environment governs survival, inflammation and autoimmunity in C9orf72LOF mice. **a**, Aseptic embryo transfer of C9orf72 neo-deleted allele from Harvard BRI to the Broad Institute. Male and female mice were aged for survival or tissue collection. CNS, central nervous system. **b, c**, Survival of mice at Harvard BRI (C9orf72^{+/+}, $n=55$; C9orf72^{+/−}, $n=114$; C9orf72^{−/−}, $n=62$) (**b**) or the Broad Institute (C9orf72^{+/+}, $n=22$; C9orf72^{+/−}, $n=36$; C9orf72^{−/−}, $n=23$) (**c**) (Gehan–Breslow–Wilcoxon). NS, not significant. **d–g**, Age-matched (48-week-old) mice reared at Harvard BRI (C9orf72^{+/+}, $n=12$; C9orf72^{+/−}, $n=13$; C9orf72^{−/−}, $n=10$) or the Broad Institute (C9orf72^{+/+}, $n=12$; C9orf72^{+/−}, $n=18$; C9orf72^{−/−}, $n=11$) were assessed for spleen weight (**d**), blood neutrophil count (**e**), blood platelet count measured at 0 °C (**f**) and plasma anti-double-stranded (ds)DNA antibody activity (**g**). In **d–g**, one-way ANOVA with Sidak's multiple comparisons. Each dot represents one mouse.

facility (hereafter referred to as C9orf72(Harvard) mice) (Fig. 1a). To assess the reproducibility of the original findings at Harvard, we aged an independent cohort of C9orf72(Harvard) mice (C9orf72(Harvard)^{+/+}, $n=55$; C9orf72(Harvard)^{+/−}, $n=114$; C9orf72(Harvard)^{−/−}, $n=62$) and again found that C9orf72(Harvard)^{+/−} mice (Gehan–Breslow–Wilcoxon $P=0.0460$) and C9orf72(Harvard)^{−/−} mice (Gehan–Breslow–Wilcoxon $P<0.0001$) were at an increased risk of premature mortality (Fig. 1b). The causes of death in these mice—which included cervical lymphadenopathy, wasting and severe ataxia—were indistinguishable from those that were observed previously⁷, and were closely tied to their underlying autoimmune condition (Extended Data Fig. 2a, b). By contrast, we observed no early mortality or motor behaviour deficit in either heterozygous or homozygous mutant mice at the Broad Institute (C9orf72(Broad)^{+/+}, $n=22$, C9orf72(Broad)^{+/−}, $n=36$, C9orf72(Broad)^{−/−}, $n=23$) (Fig. 1c, Extended Data Fig. 2c). As a result, C9orf72^{−/−} mice were significantly more likely to die prematurely when reared at Harvard than at the Broad Institute (Gehan–Breslow–Wilcoxon test, $P=0.0179$). We therefore conclude that signals from the environment can be significant modifiers of lifespan when C9orf72 function declines.

To determine whether the improved survival that we observed in C9orf72(Broad) mice was associated with a diminution of inflammatory and autoimmune endophenotypes⁷, we jointly analysed age-matched mice reared at each facility (Fig. 1d–g, Extended Data Fig. 2d, e). As previously reported⁷, C9orf72(Harvard) mice exhibited autoimmune and inflammatory phenotypes, including significantly elevated levels of IL-23, IL-10, IL-22, G-CSF, IL-17a, TNF, IFN γ , IL-1 β and IL-12p70 ($P<0.05$) (Extended Data Fig. 2e) as well as splenomegaly ($P<0.0001$) (Fig. 1d), neutrophilia ($P<0.0001$) (Fig. 1e), pseudo-thrombocytopenia ($P<0.0001$) (Fig. 1f, Extended Data Fig. 2f, g) and development of auto-antibodies ($P<0.0001$) (Fig. 1g). Notably and in every case, these inflammatory phenotypes were significantly reduced

in C9orf72(Broad)^{−/−} mice relative to their C9orf72(Harvard) mutant counterparts (Fig. 1d–g). In fact, the reduction of inflammation in the pro-survival Broad Institute environment was sufficiently reduced that many inflammatory phenotypes that we routinely observed in mutant mice at Harvard were no longer significantly different between C9orf72^{−/−} and C9orf72^{+/−} mice at the Broad Institute. It is notable that the few phenotypes that remained significantly different between C9orf72(Broad)^{−/−} and C9orf72(Broad)^{+/−} mice, such as modest splenomegaly (one-way analysis of variance (ANOVA) with Sidak's multiple comparisons, $P=0.0004$), were those that have been most widely reported^{6,13,14}. Thus, an environment that improved survival also ameliorated the underlying inflammatory and autoimmune disease found in C9orf72 mutant mice.

Antibiotics prevent inflammation

We next considered variables between the two environments that might have contributed to such marked differences in the severity of mutant phenotypes. We found that diet, light cycle and many other features of the two environments were similar. However, a review of microbial screening reports from the two facilities indicated that murine norovirus (Fisher's exact test, $P=0.0140$), *Helicobacter* spp. (Fisher's exact test, $P<0.0001$), *Pasteurella pneumotropica* (Fisher's exact test, $P=0.0070$) and *Tritrichomonas muris* (Fisher's exact test, $P<0.0001$) were significantly more common in C9orf72(Harvard) mice than in C9orf72(Broad) mice (Supplementary Table 1). It is important to note that the differences between the two colonies were well within norms for Assessment and Accreditation of Laboratory Animal Care processes. The differential components of the microflora that we found at Harvard are not generally considered pathogenic, consistent with the normal health and lifespan of control mice in that environment⁷ (Fig. 1b). However, *Helicobacter* spp. have previously been suggested to have immune-stimulating properties¹⁰, which raises the possibility that changes in gut microflora between the two environments might underlie the increased rate of mortality and inflammatory phenotypes that we found in C9orf72(Harvard) mutant mice.

To learn whether the resident microflora contributed to the inflammation and autoimmunity seen in C9orf72(Harvard) mutant mice, we weaned new C9orf72(Harvard) mice (C9orf72(Harvard)^{+/+}, $n=14$; C9orf72(Harvard)^{−/−}, $n=22$) and administered either vehicle or broad-spectrum antibiotics before the onset of inflammatory disease (day 30), then monitored related phenotypes for 200 days (Fig. 2a). As expected, antibiotics significantly reduced the abundance and diversity of bacterial species (including *Helicobacter* spp.), without affecting levels of murine norovirus. The guts of vehicle-treated control mice were largely unaltered (Fig. 2b, Extended Data Fig. 3a). We found that vehicle had no effect on the development of either inflammatory or autoimmune phenotypes in C9orf72(Harvard)^{−/−} mice, including cytokine storm (Extended Data Fig. 3b), neutrophilia (Fig. 2c), pseudo-thrombocytopenia (Fig. 2d), autoimmunity (Fig. 2e) and splenomegaly (Fig. 2f, Extended Data Fig. 3c). By contrast, providing lifelong antibiotics treatment to C9orf72(Harvard)^{−/−} mice completely suppressed the emergence of all of these phenotypes (Fig. 2c–f, Extended Data Fig. 3b–i). Thus, our experiments suggest that signals derived from gut bacteria promote inflammation and autoimmunity when C9orf72 function is diminished. However, we found that chronic administration of antibiotics resulted in previously reported health consequences (including hepatotoxicity)¹⁷, which prevented us from assessing behavioural and survival outcomes.

We next asked whether the acute suppression of gut microbiota could ameliorate inflammatory and autoimmune phenotypes after their establishment in C9orf72(Harvard) mutant mice. To this end, we obtained another independent cohort of C9orf72(Harvard) mice (C9orf72(Harvard)^{+/+}, $n=25$; C9orf72(Harvard)^{−/−}, $n=24$; day 250), demonstrated these mice displayed the expected inflammatory phenotypes

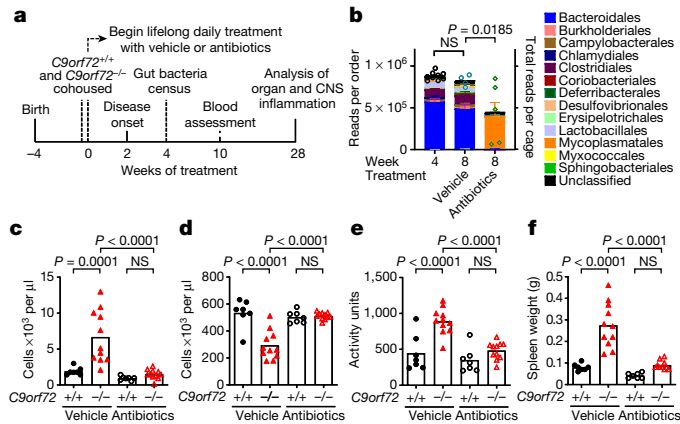


Fig. 2 | Lifelong suppression of gut microflora prevents inflammation and autoimmunity in *C9orf72*LOF mice. **a**, Male and female *C9orf72(Harvard)*^{+/+} and *C9orf72(Harvard)*^{-/-} neo-deleted mice of weaning age were cohoused by treatment group, then administered vehicle (*C9orf72(Harvard)*^{+/+}, $n=7$; *C9orf72(Harvard)*^{-/-}, $n=11$) or antibiotics (*C9orf72(Harvard)*^{+/+}, $n=7$; *C9orf72(Harvard)*^{-/-}, $n=11$) daily for life. **b–f**, Mice were assessed for gut microbial composition at 4 weeks (**b**) and blood measurements at 8 weeks (**c–e**), and killed for organ and central nervous system assessment at 28 weeks (**f**). **b**, 16S rDNA sequencing of bacteria diversity in faeces. Each dot represents total sequencing reads per cage. One-way ANOVA with Dunnett's multiple comparisons. **c**, Blood neutrophil count. **d**, Blood platelet count measured at 0 °C. **e**, Plasma anti-dsDNA antibody activity. **f**, Spleen weight. In **c–f**, one-way ANOVA with Sidak's multiple comparisons. Each dot represents one mouse.

relative to control mice and showed that they exhibited poor performance on the accelerating rotarod (Fig. 3a–d, Extended Data Fig. 4a). Then, we began acute administration of broad-spectrum antibiotics and monitored associated phenotypes over the course of 60 days. We found that this treatment significantly reduced each of the inflammatory and autoimmune phenotypes in mutant mice (Fig. 3b–d), including splenomegaly ($P=0.0002$) (Extended Data Fig. 4c, d) and improved rotarod performance ($P=0.0398$) (Extended Data Fig. 4a). By contrast, treatment with vehicle had no effect on these measures (Fig. 3b–d, Extended Data Fig. 4a–d).

Faecal transplants mitigate inflammation

To more directly investigate whether the phenotypic improvements were due to the microbial communities of the gut (rather than unrelated consequences of antibiotics treatment), we performed faecal transplant experiments. We produced another cohort of *C9orf72(Harvard)* mice (*C9orf72(Harvard)*^{+/+}, $n=27$; *C9orf72(Harvard)*^{-/-}, $n=32$; day 100) and demonstrated that these mice displayed the expected inflammatory phenotypes relative to control mice. We then suppressed the gut microflora of these mice with transient antibiotic treatment, and transplanted with faeces from either the pro-inflammatory (Harvard BRI) or pro-survival (Broad Institute) environment (Fig. 3e). Transplantation of pro-survival gut microflora significantly improved each of the inflammatory and autoimmune phenotypes (Fig. 3f–h, Extended Data Fig. 4e). By contrast, transplant with microflora from the pro-inflammatory facility did not improve these measures, which suggests that the benefits we observed when transplanting faeces from the protective environment were not merely due to the brief antibiotic treatment that enabled microbial engraftment. Therefore, our studies establish that the inflammatory and autoimmune disease that underlies premature mortality in *C9orf72(Harvard)* mutant mice can be therapeutically prevented, and that signals from particular gut microbiota help to maintain this disease.

Profiling gut bacteria

To identify the bacterial species of the gut that are associated with severe phenotypes in *C9orf72(Harvard)* mutant mice, we surveyed the composition of faeces from two pro-inflammatory environments in which the mutant mice perished^{7,12}, as well as from one previously published⁶ and one additional pro-survival environment (Fig. 3i). Principal component analysis readily separated samples from the four environments, with the largest principal component (principal component 1, 28.7% of variance) separating the two pro-inflammatory environments from the two pro-survival environments (Fig. 3j). Deeper investigation of this axis of variance revealed a shared significant decrease in α -diversity in the two pro-inflammatory environments, and unsupervised hierarchical clustering demonstrated that samples from the pro-inflammatory environments showed β -diversity disparate from that in pro-survival environments (Fig. 3k, Extended Data Fig. 5f). Exemplifying these considerable differences in community structure, 62 of 301 bacterial species we identified (20.6%) were significantly altered in their abundance when jointly comparing the two pro-survival environments to the two pro-inflammatory environments ($P<0.0002$) (Extended Data Fig. 5a–e). Consistent with initial observations (Supplementary Table 1), *Helicobacter*spp. were found in both of the pro-inflammatory environments (Extended Data Fig. 5g, h, Supplementary Fig. 1) but were absent in pro-survival environments.

We next characterized the extent of microbial reconstitution in our faecal transplant recipients (Extended Data Fig. 6a–f). Hierarchical clustering of β -diversity revealed that the microbial composition in mice that received faecal transplants from the Broad Institute environment were more similar to faeces from mice housed at the Broad Institute than to faeces from mice housed at Harvard BRI or faeces from mice that received faecal transplants from the Harvard environment (Extended Data Fig. 6d). Analysis of individual bacteria similarly supported the success of our transplants: 85% (199 out of 234) of bacterial species identified in faeces from mice housed at Harvard BRI being detected in mice that received faecal transplants from the Harvard environment, and 75% (178 out of 236) of bacterial species identified in faeces from mice housed at the Broad Institute detected in mice that received faecal transplants from the Broad Institute environment (Extended Data Fig. 6f). Semi-quantitative PCR for *Helicobacter*spp. ribosomal (r)DNA further confirmed the reconstitution of Harvard-specific microorganisms in the recipients of faecal transplants from the Harvard environment, and their elimination from the recipients of faecal transplants from the Broad Institute environment (Extended Data Fig. 5i, Supplementary Fig. 1).

Gut components regulate myeloid cytokines

To mechanistically explore how varied faecal components in separate environments alter cytokine burden and autoimmunity in *C9orf72*^{-/-} mice, we stimulated bone-marrow-derived macrophages from *C9orf72(Harvard)* mice with chemical analogues of microbial components and found that both *C9orf72(Harvard)*^{+/+} and *C9orf72(Harvard)*^{-/-} bone-marrow-derived macrophages released higher levels of several pro-inflammatory cytokines than *C9orf72(Harvard)*^{+/+} control cells in response to bacterial lipopeptide, single-stranded (ss)RNA and ssDNA (Extended Data Fig. 7a–c). Given these findings, we next asked whether faecal material from mice housed at Harvard BRI contained higher levels of innate-immune stimulating factors than faeces from mice at the Broad Institute. To this end, we individually administered normalized concentrations of faecal Eubacteria from both institutions to *C9orf72(Harvard)*^{-/-} and *C9orf72(Harvard)*^{+/+} bone-marrow-derived macrophages. We found that *C9orf72*^{-/-} bone-marrow-derived macrophages produced significantly higher levels of TNF when exposed to faecal material from Harvard BRI than when exposed to faeces from the Broad Institute (Extended Data Fig. 7d). In addition, serial dilutions

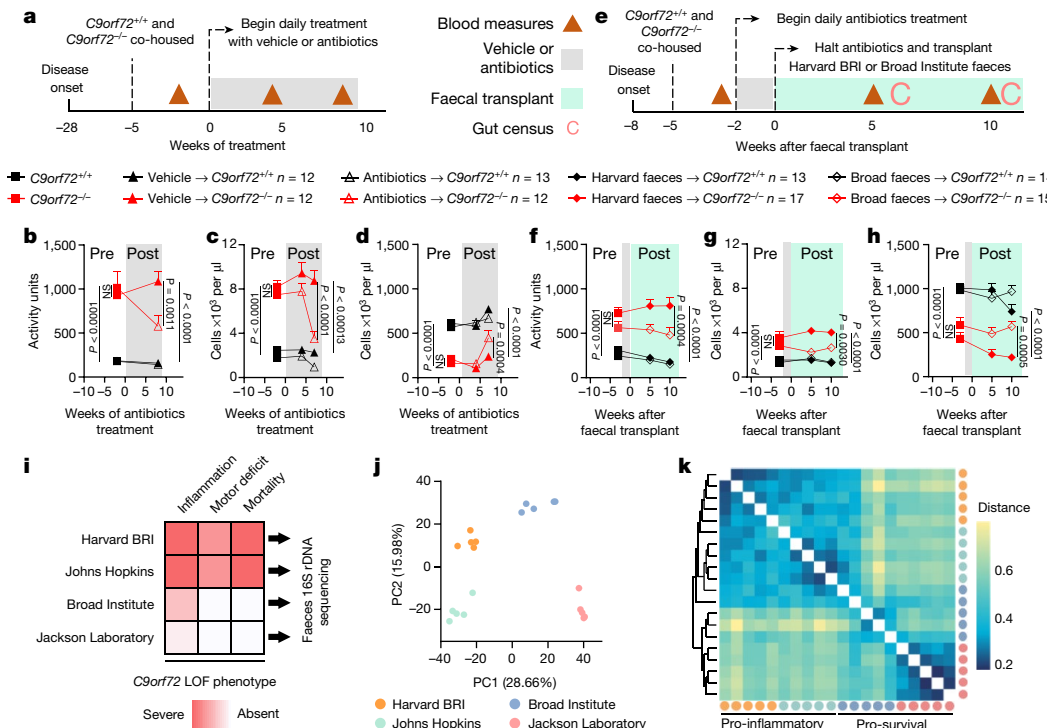


Fig. 3 | Gut bacteria propagates inflammation and autoimmunity in C9orf72LOF mice. **a**, Age-matched (36-week-old) female *C9orf72(Harvard)*^{+/+} and *C9orf72(Harvard)*^{-/-} neo-deleted mice were cohoused by treatment group, then administered vehicle (*C9orf72(Harvard)*^{+/+}, $n=12$; *C9orf72(Harvard)*^{-/-}, $n=12$) or antibiotics (*C9orf72(Harvard)*^{+/+}, $n=13$; *C9orf72(Harvard)*^{-/-}, $n=12$) daily. **b–d**, These mice were then assessed for plasma anti-dsDNA antibody activity (**b**), blood neutrophil count (**c**) and blood platelet count measured at 0 °C (**d**). **e**, Age-matched (13-week-old) female *C9orf72(Harvard)*^{+/+} and *C9orf72(Harvard)*^{-/-} neo-deleted mice were cohoused by treatment group, administered antibiotics for two weeks, and then gavaged with faeces from the Harvard BRI environment (*C9orf72(Harvard)*^{+/+}, $n=13$; *C9orf72(Harvard)*^{-/-},

$n=17$) or Broad Institute environment (*C9orf72(Harvard)*^{+/+}, $n=14$; *C9orf72(Harvard)*^{-/-}, $n=15$). **f–h**, These mice were then assessed for plasma anti-dsDNA antibody activity (**f**), blood neutrophil count (**g**) and blood platelet count measured at 0 °C (**h**). **i–k**, Faecal pellets ($n=5$ each) from two pro-inflammatory environments (Harvard BRI and Johns Hopkins) and two pro-survival environments (Broad Institute and Jackson Laboratory) were subjected to 16S rRNA sequencing (**i**), and then assessed by principal component (PC) analysis (**j**) and Bray–Curtis dissimilarity matrix of β-diversity (**k**). In **b–d**, **f–h**, one-way ANOVA with Sidak's multiple comparisons. Each dot represents one mouse.

revealed that a combination of faeces from Harvard BRI and a *C9orf72*^{-/-} genotype leads to TNF release at the lowest faecal concentrations (Extended Data Fig. 7d).

Environment governs neuro-inflammation

Neuro-inflammation is a pathological hallmark of ALS and FTD associated with mutations in *C9ORF72*^{18,19}, with substantial infiltration of peripheral immune cells noted in the spinal cord of patients with ALS^{20,21}. We used the pan-haematopoietic marker CD45 to distinguish CD45^{mid} resident microglia from peripherally derived CD45^{high} cells²² and found that infiltrating cells were present at sites of focal inflammation within the spinal cord parenchyma of *C9orf72(Harvard)*^{-/-} mice (Fig. 4a, Extended Data Fig. 8a–h, Supplementary Videos 1, 2). Mass cytometry analysis revealed that the CD45^{high} cells that infiltrated the spinal cord were mostly CD11b⁺Ly6C⁺Ly6G⁺CD39⁻ neutrophils and CD3e⁺ T cells (Extended Data Fig. 8a–f; gating strategy is in Supplementary Information). Notably, lifelong suppression of gut microbiota with antibiotics prevented the accumulation of infiltrating myeloid cells within the spinal cord of *C9orf72(Harvard)*^{-/-} mice (Fig. 4b, c).

In addition to infiltrating peripheral immune cells, there are also substantial changes to resident microglia in the nervous systems of patients with ALS or FTD²³. Previous studies^{6,8,9,24} have implicated *C9orf72* and its interactor SMCR8 in regulation of endolysosomal trafficking and autophagy, particularly in myeloid derivatives. We found that

microglia from the spinal cord of *C9orf72(Harvard)*^{-/-} mice expressed higher levels of the lysosome-associated proteins LAMP1⁶ (Extended Data Fig. 9a, Supplementary Videos 3, 4) and cathepsin B (Extended Data Fig. 9b, Supplementary Videos 5, 6). Lifelong suppression of gut microbiota did not significantly decrease LAMP1 or cathepsin B levels in *C9orf72(Harvard)*^{-/-} microglia (Extended Data Fig. 9c, d), which suggests that *C9orf72* regulates lysosomal constituents independently from microbial signals.

To examine the activation status of resident microglia in *C9orf72(Harvard)* mutant mice and to ask whether microglial activation might be altered by signals from the microbiota, we measured levels of the pattern recognition receptor dectin 1, the chemokine receptor CCR9 and the lipoprotein lipase LPL, which have previously been associated with pro-inflammatory microglial states^{25–27}. Consistent with the notion that microglia become activated when *C9orf72* levels decline, we found that dectin 1 and CCR9 were enriched in microglia from *C9orf72(Harvard)*^{-/-} mice (Fig. 4d–f, Extended Data Fig. 9e–g, Supplementary Videos 7, 8). Importantly, dectin 1 and CCR9 expression were significantly reduced in microglia from *C9orf72(Harvard)* mutant mice with gut microbiota that was chronically suppressed with antibiotics (Fig. 4d–f). These results demonstrate that when *C9orf72* function is reduced, peripheral immune cells can infiltrate the spinal cord, where they associate with sites of neuro-inflammation, and that treatment with antibiotics, which suppresses the microbiota, modulates both infiltration and microglial activation.

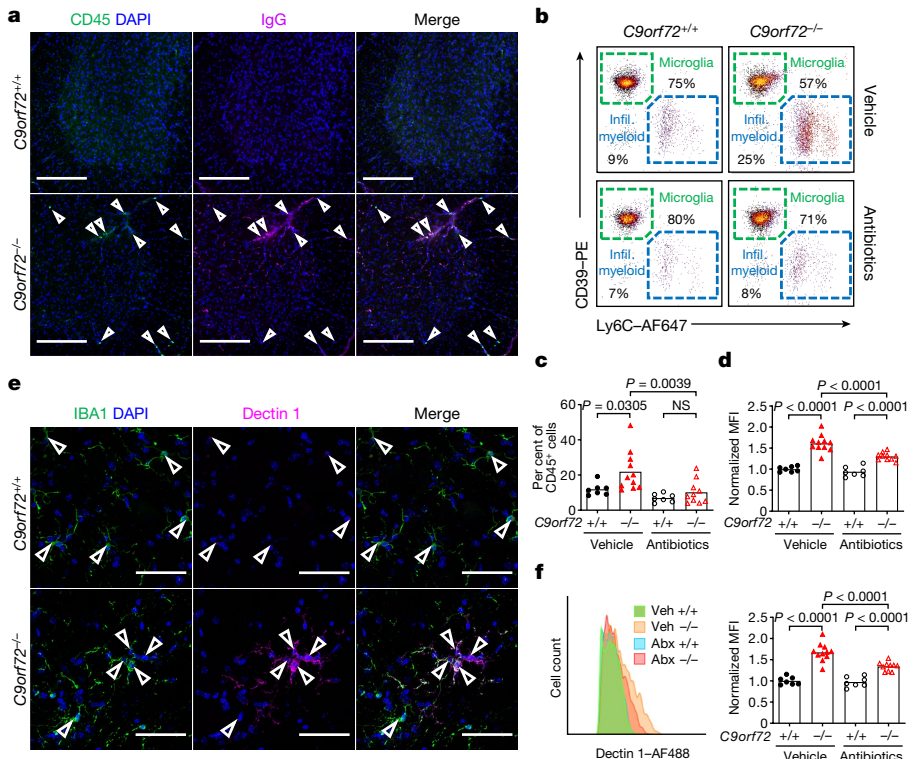


Fig. 4 | Gut microflora promotes myeloid cell infiltration and microgliosis in *C9orf72*LOF spinal cord. **a**, Orthogonal projection of CD45 and mouse immunoglobulin G (IgG) in lumbar spinal cord of 55-week-old *C9orf72*(Harvard) neo-deleted mice (*C9orf72*(Harvard)^{+/+}, $n=3$; *C9orf72*(Harvard)^{-/-}, $n=3$), showing cells infiltrating the lumbar spinal cord. Scale bars, 200 μ m. **b**, Representative gating of CD45⁺CD11b⁺ cells from spinal cord of *C9orf72*(Harvard) mice in Fig. 2. Infil., infiltrating. **c**, Quantification of CD45^{high}CD11b⁺Ly6C⁺ myeloid cells infiltrating the spinal cord, shown in **b**. **d**, Quantification of CCR9 expression on CD45^{mid}CD11b⁺CD39⁺ microglia from

the spinal cord of *C9orf72*(Harvard) mice, shown in Fig. 2. MFI, mean fluorescence intensity. **e**, Orthogonal projection of dectin 1 in IBA1⁺ microglia in lumbar spinal cord from 55-week-old *C9orf72*(Harvard) neo-deleted mice (*C9orf72*(Harvard)^{+/+}, $n=3$; *C9orf72*(Harvard)^{-/-}, $n=3$). Scale bars, 50 μ m. **f**, Dectin 1 in CD45^{mid}CD11b⁺CD39⁺ microglia from spinal cord of *C9orf72*(Harvard) mice in Fig. 2. +/+, *C9orf72*(Harvard)^{+/+}; -/-, *C9orf72*(Harvard)^{-/-}; abx, antibiotics-treated; veh, vehicle-treated. In **c**, **d**, **f**, one-way ANOVA with Sidak's multiple comparisons. Each dot represents one mouse.

Discussion

Our results indicate that when *C9orf72* function declines, the environment generally—and the gut microbiota specifically—become potent modifiers of whether autoimmunity, neural inflammation, motor deficits and premature mortality occur. The effect of environment and accompanying changes in microbial microflora are so strong in this mouse model that in one environment, inflammatory disease and death were highly penetrant phenotypes, whereas in another they were essentially absent. We therefore provide the probable explanation for the considerable phenotypic variation that has been observed across groups studying this *C9orf72*LOF allele in mice^{6,7,12,13}. These conclusions are important because they re-emphasize that the 50% reduction in the levels of *C9ORF72* found in patients with ALS or FTD who have mutations in *C9ORF72* are a credible cause for the neural inflammation that are characteristic in their condition. Most provocatively, our findings also suggest that variance in microbiota could explain why some carriers of the *C9ORF72* mutation develop ALS or FTD, or overt inflammatory conditions such as lupus^{15,16}, while others do not.

It should be re-emphasized that the microorganisms present in the environments we studied here are not considered mouse pathogens per se, and that their abundances were within the scope found in comparable institutions²⁸. Importantly, the environmental conditions that triggered severe phenotypes in our *C9orf72*(Harvard) mice were reproducible elsewhere. Previous reports^{7,12} have noted a relationship between the reduction in *C9orf72* function and an increased rate of premature mortality comparable to that described here. It is notable

that these two pro-inflammatory environments were most similar in their microbial constituents and also shared many microorganisms that were not present in the two pro-survival locations we surveyed. Given the large number of species that we found significantly differ in their abundance between pro-inflammatory and pro-survival environments (Fig. 3i, Extended Data Fig. 5c), future studies will be needed to elucidate the relative contribution of individual bacterial species to variation in the inflammatory and autoimmune phenotypes we report here. However, microorganism-by-microorganism analysis of varying environments and our transplant mice would seem to rule out the previously reported protective effects of *Akkermansia muciniphila*^{29,30} (Extended Data Fig. 6f) and potential inflammatory influences of *T. muris* (Extended Data Fig. 5e).

It is increasingly appreciated that gut microorganisms alter the maturation and function of microglia³¹, can influence the activity of neurons in the central nervous system³² and contribute to neuro-inflammation and neuropathology in models of Alzheimer's³³ and Parkinson's disease³⁴. However, only initial surveys of the gut microbiota have been reported in patients with neurological conditions³⁵ and, thus far, results from initial studies in patients with ALS have been mixed^{36,37}. One study has reported significant differences between the microbial constituents of patients with ALS and controls³⁶, whereas another found no clear distinctions³⁷. Given the genetic heterogeneity exhibited within patients with ALS, it is perhaps not surprising that early studies have not reached consensus.

Consistent with the idea there are complex interactions between the germline genotype of a patient and their gut microflora in ALS, it

was recently reported that *SOD1*-transgenic mice displayed a faster decline when bacterial load was reduced, which was linked to reduced bacterial production of nicotinamide²⁹. Although we cannot rule out the presence of protective microorganisms in some environments, our studies suggest that lowering the bacterial load in *C9orf72*-mutant mice was in aggregate protective, probably by reducing the exposure of their genetically sensitized innate immune response to inflammatory factors derived from microorganisms. In sum, our studies suggests that the microbiome may be an important governor of the onset and progression of neurological disease in patients with *C9ORF72* mutations, including those experiencing autoimmunity and inflammatory conditions before a diagnosis of ALS or FTD^{15,16}. To test this idea, a key future experiment will be to identify *C9ORF72* repeat expansion carriers within families known to be predisposed to developing ALS or FTD, and to determine whether the gut microbiota differs between individuals that remain healthy and those that acquire the conditions.

Online content

Any methods, additional references, Nature Research reporting summaries, source data, extended data, supplementary information, acknowledgements, peer review information; details of author contributions and competing interests; and statements of data and code availability are available at <https://doi.org/10.1038/s41586-020-2288-7>.

1. DeJesus-Hernandez, M. et al. Expanded GGGGCC hexanucleotide repeat in noncoding region of *C9ORF72* causes chromosome 9p-linked FTD and ALS. *Neuron* **72**, 245–256 (2011).
2. Majounie, E. et al. Frequency of the *C9orf72* hexanucleotide repeat expansion in patients with amyotrophic lateral sclerosis and frontotemporal dementia: a cross-sectional study. *Lancet Neurol.* **11**, 323–330 (2012).
3. Mori, K. et al. The *C9orf72* GGGGCC repeat is translated into aggregating dipeptide-repeat proteins in FTLD/ALS. *Science* **339**, 1335–1338 (2013).
4. Ash, P. E. A. et al. Unconventional translation of *C9ORF72* GGGGCC expansion generates insoluble polypeptides specific to c9FTD/ALS. *Neuron* **77**, 639–646 (2013).
5. Donnelly, C. J. et al. RNA toxicity from the ALS/FTD *C9ORF72* expansion is mitigated by antisense intervention. *Neuron* **80**, 415–428 (2013).
6. O'Rourke, J. G. et al. *C9orf72* is required for proper macrophage and microglial function in mice. *Science* **351**, 1324–1329 (2016).
7. Burberry, A. et al. Loss-of-function mutations in the *C9ORF72* mouse ortholog cause fatal autoimmune disease. *Sci. Transl. Med.* **8**, 347ra93 (2016).
8. Nassif, M., Woehlbier, U. & Manque, P. A. The enigmatic role of *C9ORF72* in autophagy. *Front. Neurosci.* **11**, 442 (2017).
9. Shi, Y. et al. Haploinsufficiency leads to neurodegeneration in *C9ORF72* ALS/FTD human induced motor neurons. *Nat. Med.* **24**, 313–325 (2018).
10. Whary, M. T. & Fox, J. G. Natural and experimental *Helicobacter* infections. *Comp. Med.* **54**, 128–158 (2004).
11. Flannigan, K. L. & Denning, T. L. Segmented filamentous bacteria-induced immune responses: a balancing act between host protection and autoimmunity. *Immunology* **154**, 537–546 (2018).
12. Ugolini, J. et al. Loss of *C9orf72* enhances autophagic activity via deregulated mTOR and TFEB signaling. *PLoS Genet.* **12**, e1006443 (2016).
13. Jiang, J. et al. Gain of toxicity from ALS/FTD-linked repeat expansions in *C9ORF72* is alleviated by antisense oligonucleotides targeting GGGGCC-containing RNAs. *Neuron* **90**, 535–550 (2016).
14. Atanasio, A. et al. *C9orf72* ablation causes immune dysregulation characterized by leukocyte expansion, autoantibody production, and glomerulonephropathy in mice. *Sci. Rep.* **6**, 23204 (2016).
15. Miller, Z. A. et al. Increased prevalence of autoimmune disease within C9 and FTD/MND cohorts. *Neuroimmunol. Neuroinflamm.* **3**, e301 (2016).
16. Fredi, M. et al. *C9orf72* intermediate alleles in patients with amyotrophic lateral sclerosis, systemic lupus erythematosus, and rheumatoid arthritis. *Neuromolecular Med.* **21**, 150–159 (2019).
17. Stine, J. G. & Lewis, J. H. Hepatotoxicity of antibiotics: a review and update for the clinician. *Clin. Liver Dis.* **17**, 609–642, ix (2013).
18. Ransohoff, R. M. How neuroinflammation contributes to neurodegeneration. *Science* **353**, 777–783 (2016).
19. McCauley, M. E. & Baloh, R. H. Inflammation in ALS/FTD pathogenesis. *Acta Neuropathol.* **137**, 715–730 (2019).
20. Zhao, W., Beers, D. R. & Appel, S. H. Immune-mediated mechanisms in the pathoproteinosis of amyotrophic lateral sclerosis. *J. Neuroimmune Pharmacol.* **8**, 888–899 (2013).
21. Zondler, L. et al. Peripheral monocytes are functionally altered and invade the CNS in ALS patients. *Acta Neuropathol.* **132**, 391–411 (2016).
22. Zhang, G. X., Li, J., Ventura, E. & Rostami, A. Parenchymal microglia of naïve adult C57BL/6J mice express high levels of B7.1, B7.2, and MHC class II. *Exp. Mol. Pathol.* **73**, 35–45 (2002).
23. Lall, D. & Baloh, R. H. Microglia and *C9orf72* in neuroinflammation and ALS and frontotemporal dementia. *J. Clin. Invest.* **127**, 3250–3258 (2017).
24. Zhang, Y. et al. The *C9orf72*-interacting protein Smcr8 is a negative regulator of autoimmunity and lysosomal exocytosis. *Genes Dev.* **32**, 929–943 (2018).
25. Li, H. et al. Different neurotropic pathogens elicit neurotoxic CCR9- or neurosupportive CXCR3-expressing microglia. *J. Immunol.* **177**, 3644–3656 (2006).
26. Krasemann, S. et al. The TREM2-APOE pathway drives the transcriptional phenotype of dysfunctional microglia in neurodegenerative diseases. *Immunity* **47**, 566–581.e9 (2017).
27. Keren-Shaul, H. et al. A unique microglia type associated with restricting development of Alzheimer's disease. *Cell* **169**, 1276–1290.e17 (2017).
28. Nilsson, H.-O. et al. High prevalence of *Helicobacter* species detected in laboratory mouse strains by multiplex PCR-denaturing gradient gel electrophoresis and pyrosequencing. *J. Clin. Microbiol.* **42**, 3781–3788 (2004).
29. Blacher, E. et al. Potential roles of gut microbiome and metabolites in modulating ALS in mice. *Nature* **572**, 474–480 (2019).
30. Zhai, R. et al. Strain-specific anti-inflammatory properties of two *Akkermansia muciniphila* strains on chronic colitis in mice. *Front. Cell. Infect. Microbiol.* **9**, 239 (2019).
31. Erny, D. et al. Host microbiota constantly control maturation and function of microglia in the CNS. *Nat. Neurosci.* **18**, 965–977 (2015).
32. Olson, C. A. et al. The gut microbiota mediates the anti-seizure effects of the ketogenic diet. *Cell* **173**, 1728–1741.e13 (2018).
33. Harach, T. et al. Reduction of Abeta amyloid pathology in APPPS1 transgenic mice in the absence of gut microbiota. *Sci. Rep.* **7**, 41802 (2017).
34. Sampson, T. R. et al. Gut microbiota regulate motor deficits and neuroinflammation in a model of Parkinson's disease. *Cell* **167**, 1469–1480.e12 (2016).
35. Tremlett, H., Bauer, K. C., Appel-Cresswell, S., Finlay, B. B. & Waubant, E. The gut microbiome in human neurological disease: a review. *Ann. Neurol.* **81**, 369–382 (2017).
36. Fang, X. et al. Evaluation of the microbial diversity in amyotrophic lateral sclerosis using high-throughput sequencing. *Front. Microbiol.* **7**, 1479 (2016).
37. Brenner, D. et al. The fecal microbiome of ALS patients. *Neurobiol. Aging* **61**, 132–137 (2018).

Publisher's note Springer Nature remains neutral with regard to jurisdictional claims in published maps and institutional affiliations.

© The Author(s), under exclusive licence to Springer Nature Limited 2020

Methods

Mice

All experimental procedures were approved by the Institutional Animal Care and Use Committee of Harvard University and the Broad Institute, and were in compliance with all relevant ethical regulations. The KOMP and neo-deleted *C9orf72* loss of function strains were generated as previously described⁷. Mice were housed with nestlet bedding, red hut for enrichment, provided water ad libitum and fed ad libitum either with Prolab Isopro RMH 3000 (Harvard BRI) or with PicoLab Rodent Diet 20 (Broad Institute) and kept on a 12-h light–dark cycle. Embryo re-derivation was performed by collecting embryos from super-ovulated *C9orf72^{+/−}* females, washing embryos, then surgical transfer using an aseptic technique into the reproductive tract of pseudopregnant recipient females. For experiments involving antibiotics, mice were cohoused for at least a week before initiation of dosing. Mice were administered either vehicle (water) or a freshly prepared cocktail of four antibiotics including ampicillin sodium salt (200 mg/kg/d), neomycin trisulfate salt hydrate (200 mg/kg/d), metronidazole (200 mg/kg/d), and vancomycin hydrochloride from *Streptomyces orientalis* (100 mg/kg/d) (all from Sigma) administered by twice daily gavage. The number (*n*), sex and ages of the mice used in each study are described in figure legends or text. Power calculations (G*Power 3.1.9.2) using the mean and standard error of endophenotype data was used to estimate necessary cohort sizes for antibiotics and faecal transplant studies. Before administration of antibiotics, mice were assessed for systemic inflammatory measures and mice were allocated into groups so that no significant differences were present before treatment initiation.

Motor behaviour

Naive mice were trained on the rotarod at constant speed of 4 rpm for 300 s at least 1 d before competitive assessment. For performance trials, the rotarod accelerated from 4 to 40 rpm over 300 s using Ugo Basile mouse RotaRod NG (Harvard FAS BRI) or Panlab Rota Rod (Broad Institute). Each trial day consisted of 3 tests per mouse, with each test separated by at least 20 min. The operator was blinded to mouse genotype during trials.

Faecal transplantation

Using sterilized forceps, donor faecal pellets were collected directly from the anus, or donor upper and lower intestinal contents were isolated from euthanized mice and immediately frozen on dry ice. Recipient mice received antibiotics twice daily by gavage for two weeks, then a two day secession of antibiotics, then faecal transplantation once per day for two days. Faecal pellets and intestinal contents from donor mice were weighed, pooled, diluted to 200 mg/ml in degassed PBS and administered by oral gavage to recipient mice at 2 mg faeces per g of body weight. All cage changes were performed in HEPA filtered hoods with freshly autoclaved cages, bedding and enrichment.

Blood and cytokine measures

Peripheral blood was collected via mandible puncture into EDTA-coated tubes. Blood counts were assessed using a Hemavet (Abaxis). Samples were then centrifuged to pellet cells and plasma was collected from the supernatant. Plasma was diluted 1:2 for luminex-based multiplexed fluorescence assay to assess 36 cytokines and chemokines. Plasma was diluted 1:200 to assess mouse anti-dsDNA total IgG autoantibodies (Alpha Diagnostic International).

Tissue preparation

Mice were anaesthetized with isoflurane followed by transcardial perfusion with HBSS supplemented with 10 U/ml heparin. Spleens were dissociated by repeated trituration with a glass pipetman in HBSS, subjected to 10-min RBC lysis (eBioscience), washed in autoMACS

(Miltenyi), filtered (40 µm) and counted using a Countess (Invitrogen) for antibody staining. For flow cytometry and mass cytometry of the central nervous system, spinal cords were digested by papain and DNase diluted in EBSS (Worthington) for 10 min at 37 °C, triturated with a glass pipetman to generate large tissue chunks, and then allowed to digest for 20 min at 37 °C. DMEM supplemented with glutamax was added, samples triturated to single cells, ovomucoid (Worthington) and DNase diluted in EBSS added to inhibit protease activity, cells filtered, washed in autoMACS buffer, and pelleted at 500g for 15 min at 4 °C. Cell pellets were brought up in isotonic Percoll Plus (Sigma) diluted to 30% in autoMACS and spun for 15 min at room temperature with no brake. Floating myelin was gently removed using plastic transfer pipette. Cell pellets were resuspended, filtered, washed in autoMACS and re-pelleted at 4 °C. Cells were fixed in 4% paraformaldehyde (PFA) (Electron Microscopy Sciences) either before or after antibody staining depending on need. Samples were collected on a BD LSRII or Helios mass cytometer. Data were analysed using FlowJo and/or Cyto bank. For immunofluorescence experiments, following HBSS perfusion, mice were perfused with 4% PFA and central nervous system tissue was post-fixed in 4% PFA overnight at 4 °C. The next day, samples were washed with PBS overnight at 4 °C. Tissue was submerged in 30% sucrose for 2 d. After cryoprotection, lumbar regions were mounted in OCT and cryostat-sectioned at 30 µm.

Immunofluorescence

Spinal cord sections were washed three times in PBS to remove residual OCT. Sections were incubated in a blocking solution (10% donkey serum, 0.1M glycine, 0.1% Tween20 or 0.3% Triton X100, PBS, Image-iT FX Signal Enhancer (Thermo)) for 1 h at room temperature. Following blocking, sections were incubated with primary antibodies for 2 d on a rocker at 4 °C. Primary antibodies include: rat CD11b–FITC 1:200 (M1/70, BioLegend), rabbit cathepsin B 1:400 (D1C7Y CST), rat CD45–488 1:200 (30-F11 BioLegend), guinea pig IBA11:500 (234004 Synaptic Systems), rat LAMP11:200 (1D4B SCB), rat CCR9–FITC (9B1 BioLegend), rat Dectin 1/CLEC7A (mabg-mdect Invivogen) and mouse LPL (ab21356 Abcam). Sections were then washed with 0.1% Tween20 in PBS (for stains with CD11b, CD45, CCR9, and cathepsin B) or 0.3% TritonX100 in PBS (for stains with IBA1, LAMP1, CLEC7A (dectin 1) and LPL) at least 5 times. Secondary antibodies include: donkey-anti-rat-AlexaFluor-488, -mouse IgG-555, -rabbit-555, -rabbit-647, -rat-647, -guinea pig-647, all 1:500 dilution (Invitrogen), for 2 h at room temperature. Sections were washed again, and mounted on microscope slides in Fluoromount for curing overnight. Spinal cords were imaged on a ZEISS LSM700 with either a 10× and 40× objective, or an Axio scan Z.1 at 20× objective. Images were stitched and processed on ZEISS ZEN 2.6 image processing software and Bitplane Imaris 9.2. All comparative stains between control and mutant mice were acquired using identical laser and microscope settings, and images were processed with viewer blinded to genotype.

Flow cytometry

Dissociated single cells were stained in autoMACS on ice using the following antibodies (BioLegend): CD45–BV421 or APC–Cy7 1:200 (30-F11), rabbit cathepsin B 1:100 (D1C7Y CST) and goat-anti-rabbit-AlexaFluor-488 1:500 (Invitrogen), CCR9–FITC 1:200 (9B1), F4/80–PE–Cy5 1:400 (BM8), CD11b–AlexaFluor-700 1:400 (M1/70 Invitrogen), LAMP1–APC–Cy7 1:400 (1D4B), TruStain FCX 1:250 (93), CD39–PE 1:400 (Duha59), Ly6G–PE–Cy7 1:600 (1A8), Ly6C–AlexaFluor-647 (HK1.4). To retrieve the cathepsin B epitope, fixed cells were slowly permeabilized in 90% methanol before staining for cathepsin B.

16S sequencing and PCR assays for rodent infectious agents

DNA was isolated by Powersoil (Qiagen) per the manufacturer's protocol, and recovery yield and DNA quality were determined by fluorometric analysis. DNA concentration was standardized and amplified using

Article

16S rRNA primers spanning the V3 and V4 regions (Illumina). Resulting amplified PCR products were analysed on a Bioanalyzer (Agilent Technologies), and then purified and amplified with primers containing unique sample nucleotide barcodes (Illumina). PCR products were analysed with the Bioanalyzer for product quality control and also by SYBR green PCR to determine the quantity. All samples were pooled and standardized to a final concentration of 4.0 nM representation for each sample. The 16S PCR product pool was denatured with sodium hydroxide then adjusted to 4.0 pM and combined with 5% PhiX control DNA before loading onto a sequencing flow cell (Illumina) with 300-bp paired ends and a unique molecular tag for each sample. Following the sequencing run, the sequence data were separated on the basis of the nucleotide bar code, and then compared to the Greengenes database³⁸. Relative abundance, α -diversity, β -diversity and principal coordinate analysis were performed using QIIME analysis software³⁹. PCR assays for rodent infectious agents were performed as described⁴⁰.

PCR

Faecal DNA was isolated from faecal pellets using QIAamp Fast DNA Stool Mini Kit (Qiagen). *Helicobacter* spp. 16S rDNA was amplified using primers 5'-CTATGACGGTATCCGCC-3' and 5'-ATTCCACCTACCTCTCCC-3'. Total Eubacteria 16S rDNA was amplified using primers 5'-TCCTACGGGAGGCAGCAG-3' and 5'-GGACTACCAGGTATCTAATCCTGTT -3'. *T. muris* 28S rDNA was amplified using primers 5'-GCTTTGCAAGCTAGGTCCC-3' and 5'-TTTCTGATGGGGCGTACAC -3'. RNA was isolated from tissue by dissociating cortex in Trizol LS (Thermo) using a pellet pestle and reverse transcriptase with iScript (Biorad). Quantitative PCR with reverse transcription as performed using SYBR (Biorad). *Ly6c* was amplified using primers 5'-TACTGTGTGCAGAAAGAGCTCAG-3' and 5'-TTCCTCTTGAGAGTCCTCAATC-3'. *Gapdh* was amplified using primers 5'-TGCGACTTCAACAGCAACTC-3' and 5'-GCCTCTC TTGCTCAGTGTCC-3'.

Bone-marrow-derived macrophages

Two femurs and tibias were stripped of musculature, flushed and cultured in IMDM supplemented with 10% FCS, NEAA, glutamax, penicillin-streptomycin and 20 ng/ml mouse M-CSF (PeproTech). The medium was changed on day 3 and cells plated for experiments after 6 days. Cells were plated at 4×10^4 cells per well of a 96-well plate, and allowed to attach overnight, followed by stimulation with microbial moieties (Invivogen), including Pam3csk4 (10–1,000 ng/ml; tlrl-pms), zymosan (1 μ g/ml; tlrl-zyn), HMW poly(I:C) (10 μ g/ml; tlrl-pic), LPS (10 ng/ml; tlrl-peklps), R848 (20 ng/ml; tlrl-r848), CpG ODN (25 μ g/ml; tlrl-1826) or PGN (20 μ g/ml; tlrl-pgnb3). For faecal stimulations, previously frozen faeces were thawed, diluted to 200 mg/ml in PBS, passed through a 40- μ m filter, quick spun, and supernatant was collected and kept on ice. Bacterial DNA was isolated from each sample using QIAamp Fast DNA Stool Mini Kit (Qiagen) and total Eubacteria 16S rDNA abundance determined by qPCR. The more concentrated sample was diluted in PBS to normalize the relative Eubacteria abundance, which was confirmed

again by bacterial DNA isolation and qPCR. Dilution curves were prepared for each normalized faecal sample and added to macrophage cultures. Penicillin–streptomycin was added to cultures after 2 h, then the medium was collected after 18 h for testing by TNF enzyme-linked immunosorbent assay at 1:2 and 1:10 dilution (BioLegend).

Statistics

Statistical calculations were performed using GraphPad prism 8.0. Tests between two groups used a two-tailed Student's *t*-test. A Bonferroni-corrected *t*-test was used to assess differentially abundant bacterial species between pro-inflammatory and pro-survival environments. Tests between multiple groups used one-way ANOVA with either Tukey's or Sidak's multiple comparisons. Tests between multiple groups over time used two-way ANOVA with Dunnett's multiple comparisons. Survival curves were evaluated by generalized Wilcoxon test.

Reporting summary

Further information on research design is available in the Nature Research Reporting Summary linked to this paper.

Data availability

The 16S rDNA sequencing dataset are available through the Gene Expression Omnibus repository at GSE147325. All other data generated or analysed are included in the published Article and its Supplementary Information.

38. DeSantis, T. Z. et al. Greengenes, a chimera-checked 16S rRNA gene database and workbench compatible with ARB. *Appl. Environ. Microbiol.* **72**, 5069–5072 (2006).
39. Caporaso, J. G. et al. QIIME allows analysis of high-throughput community sequencing data. *Nat. Methods* **7**, 335–336 (2010).
40. Henderson, K. S. et al. Efficacy of direct detection of pathogens in naturally infected mice by using a high-density PCR array. *J. Am. Assoc. Lab. Anim. Sci.* **52**, 763–772 (2013).

Acknowledgements Support to K.E. was provided by The Merkin Fund at the Broad Institute, Target ALS, NIH 5R01NS089742, Harvard Stem Cell Institute and UCB. A.B. was supported by NIH 5K99AG057808-02. M.F.W. was supported by NIH 1K99MH119327-01. We thank J. Wang for providing faeces from mice housed Johns Hopkins University.

Author contributions A.B., M.F.W., J.M. and K.E. conceived the study. Experiments were performed by A.B. (Figs. 1–4, Extended Data Figs. 1–9), F.L. (Fig 1, Extended Data Fig. 2), M.F.W. (Fig. 1, Extended Data Fig. 2), K.S.S. (Fig. 4, Extended Data Figs. 8, 9), A.C. (Figs. 2–4, Extended Data Figs. 3–9), J.M. (Figs. 1–3, Extended Data Figs. 2–6, 8), N.v.G. (Extended Data Fig. 2), J.-Y.W. (Fig. 4, Extended Data Fig. 8), J.K. and G.G. (Extended Data Fig. 8), and M.Q. and P.E. and C.C. (Figs. 2, 3, Extended Data Figs. 3, 4, 8), A.B., F.L., K.S.S., J.K., G.G., N.v.G., J.-Y.W., O.P., I.K., D.T.S. and K.E. interpreted results. A.B. and K.E. wrote the manuscript.

Competing interests K.E. is a co-founder of Q-State Biosciences, Quralis and Enclear Therapies.

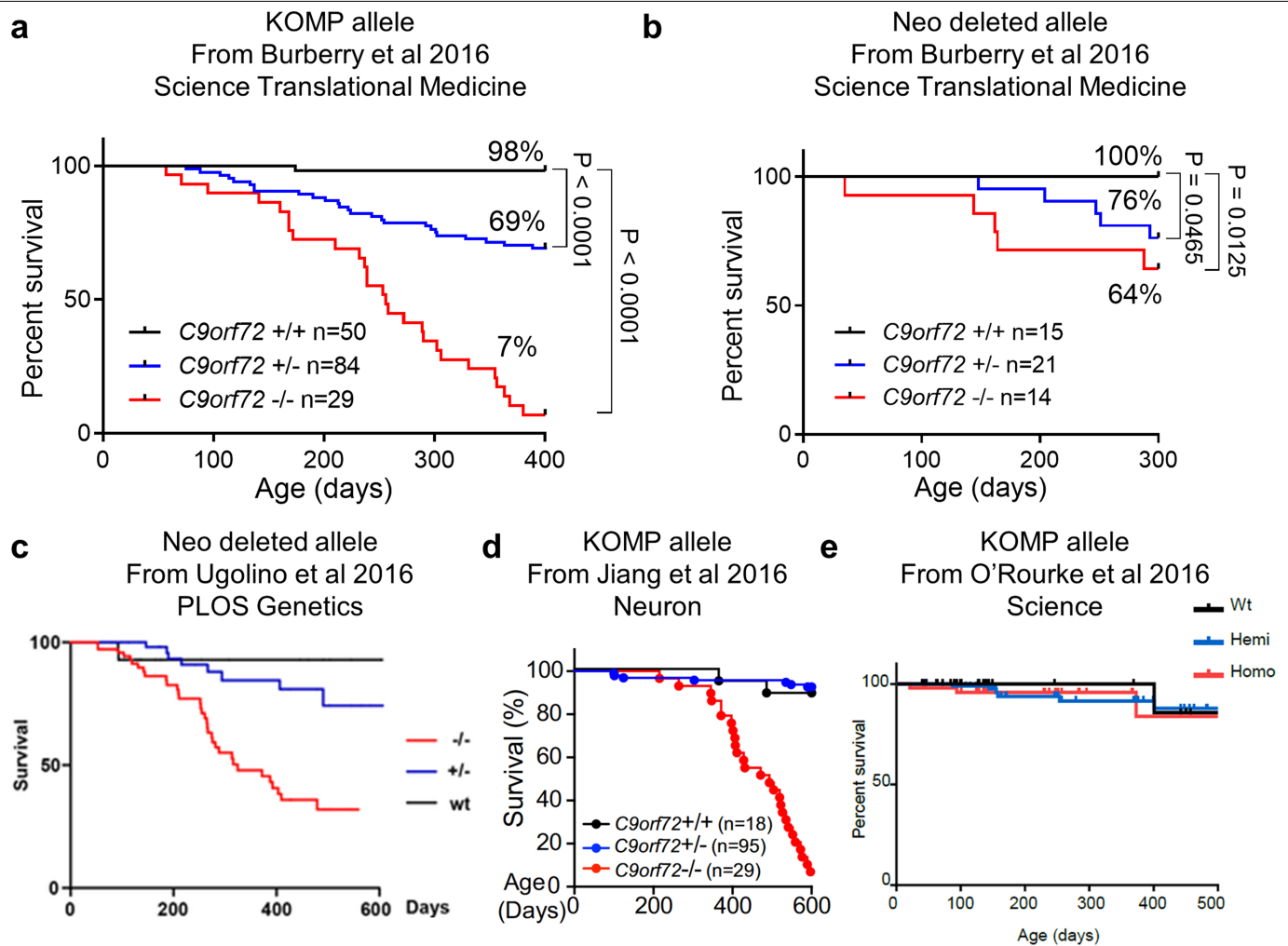
Additional information

Supplementary information is available for this paper at <https://doi.org/10.1038/s41586-020-2288-7>.

Correspondence and requests for materials should be addressed to K.E.

Peer review information *Nature* thanks Michael Fischbach, Aaron D. Gitler and the other, anonymous, reviewer(s) for their contribution to the peer review of this work.

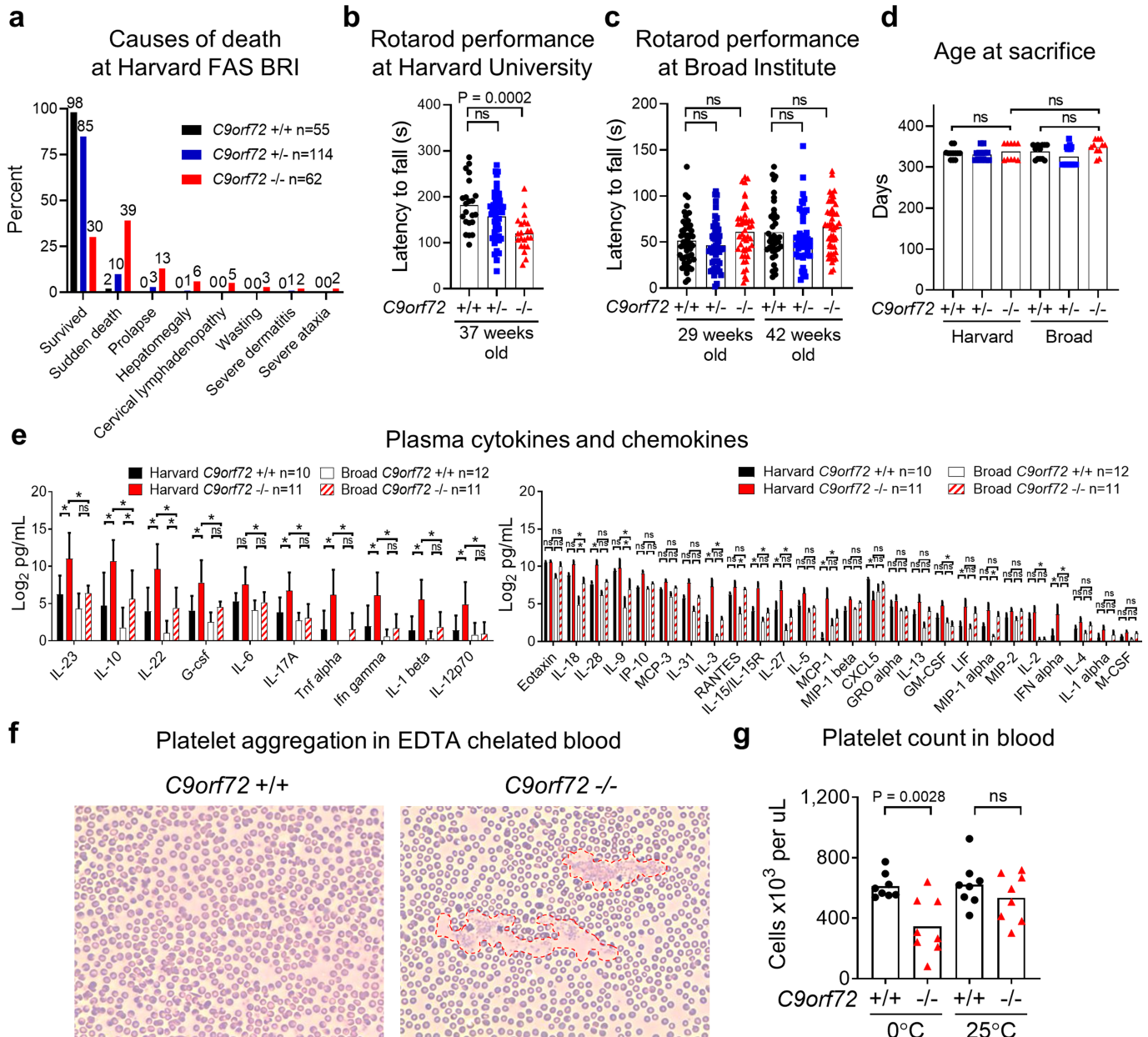
Reprints and permissions information is available at <http://www.nature.com/reprints>.



Extended Data Fig. 1 | Previously published *C9orf72* LOF survival studies.
a, From ref.⁷. Reproduced with permission from AAAS. **b**, From ref.⁷. Reproduced with permission from AAAS. **c**, Reproduced from ref.¹², licensed

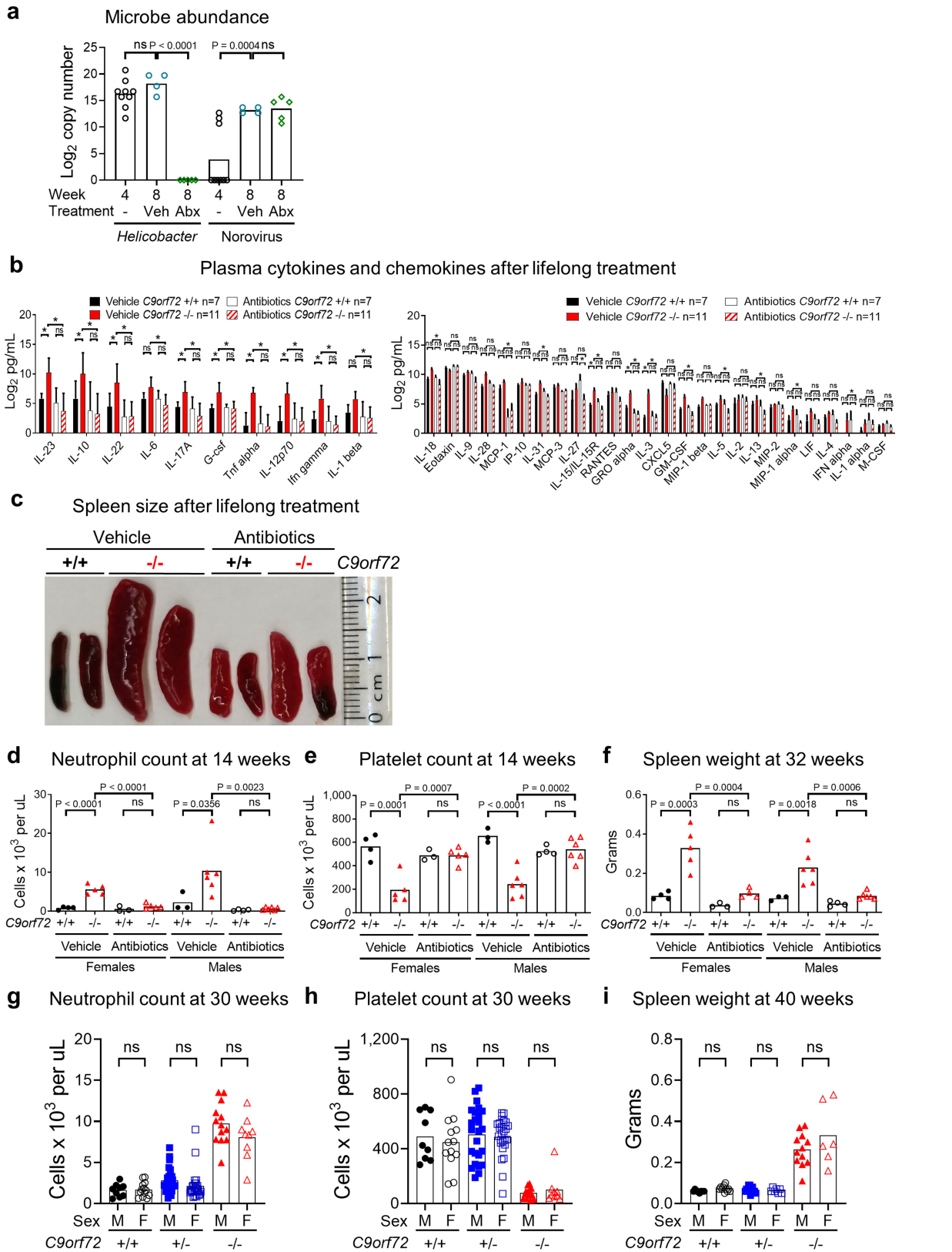
under a CC BY 4.0 licence. **d**, Reprinted from ref.¹³, with permission from Elsevier. **e**, From ref.⁶. Reproduced with permission from AAAS.

Article



Extended Data Fig. 2 | Causes of death, motor performance, levels of plasma cytokines and identification of pseudothrombocytopenia in *C9orf72*LOF mice. **a**, Causes of death or premature mortality of *C9orf72*(Harvard) mice in Fig. 1b. **b**, Accelerating rotarod performance of 37-week-old *C9orf72*(Harvard) neo-deleted mice (*C9orf72*(Harvard)^{+/+}, *n* = 22; *C9orf72*(Harvard)^{+/−}, *n* = 50; *C9orf72*(Harvard)^{−/−}, *n* = 22). **c**, Accelerating rotarod performance of *C9orf72*(Broad) neo-deleted mice at 29 weeks of age (*C9orf72*(Broad)^{+/+}, *n* = 53; *C9orf72*(Broad)^{+/−}, *n* = 52; *C9orf72*(Broad)^{−/−}, *n* = 48) or 42 weeks of age (*C9orf72*(Broad)^{+/+}, *n* = 38; *C9orf72*(Broad)^{+/−}, *n* = 48; *C9orf72*(Broad)^{−/−}, *n* = 48). In **b**, **c**, one-way ANOVA with Dunnett's multiple comparisons. Each point represents the average of three trials per mouse.

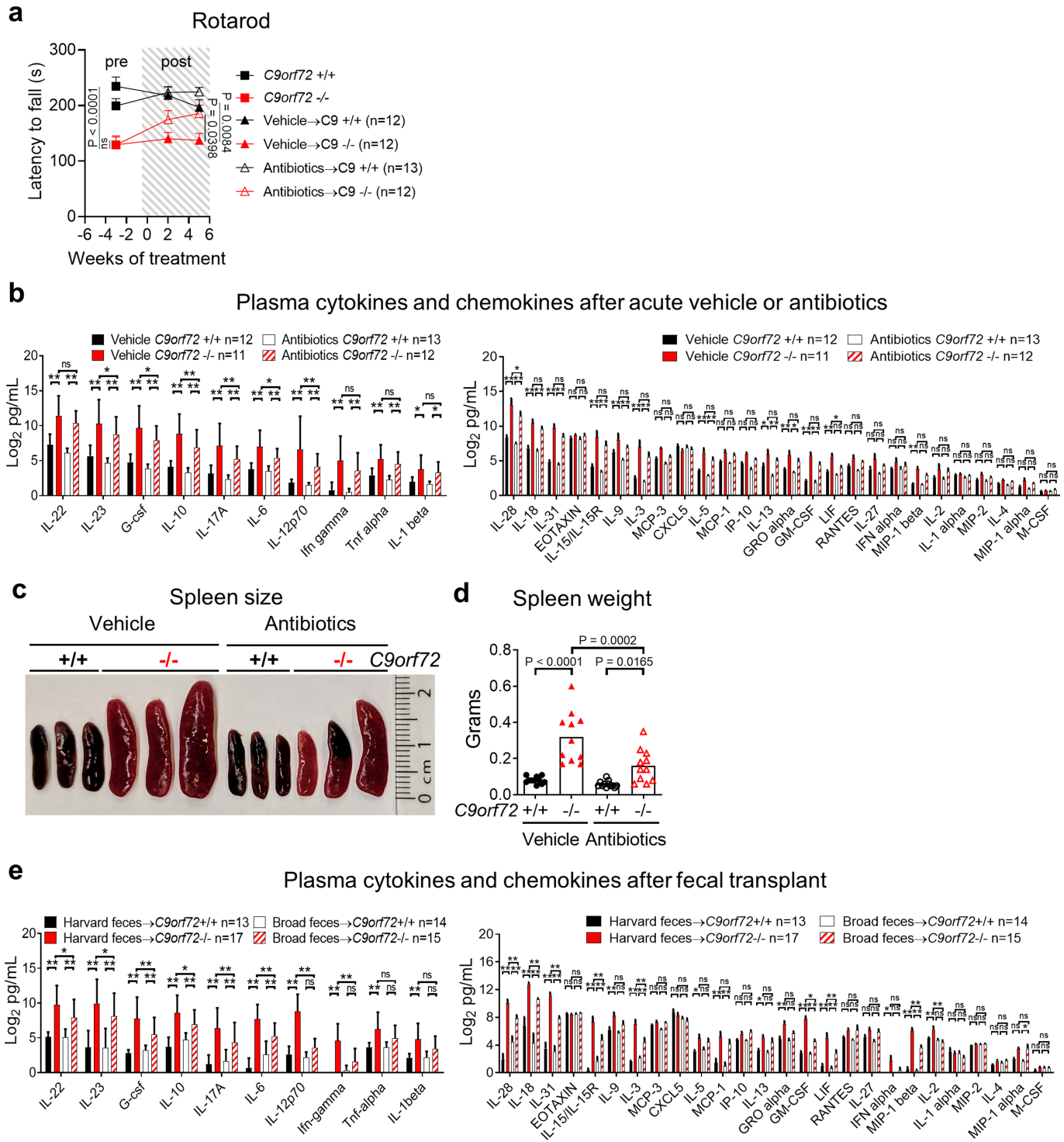
d, Age at which mice in Fig. 1d–g were killed. One-way ANOVA with Sidak's multiple comparisons. **e**, Plasma cytokines and chemokines at death from mice in Fig. 1d–g. Mean ± s.d. Two-way ANOVA with Tukey's multiple comparisons. **f**, Peripheral blood smear of 18-week-old *C9orf72*(Harvard) neo-deleted mice. Platelets from *C9orf72*(Harvard)^{−/−} mice were prone to aggregate (outlined by red dashed lines) in the presence of EDTA at 0 °C. **g**, Pseudothrombocytopenia could be reversed by warming the blood to room temperature. The reduced platelet count in the *C9orf72*(Harvard)^{−/−} model therefore represents an indirect measure of anti-platelet auto-antibodies, rather than a reduction in platelet abundance. Two-way ANOVA with Tukey's multiple comparisons. Each dot represents one mouse.



Extended Data Fig. 3 | Cytokines and chemokines in lifelong-antibiotic-treated C9orf72LOF mice and sex stratification of inflammatory phenotypes. **a**, PCR analysis of *Helicobacter* spp. and norovirus DNA in faecal pellets. Each dot represents faeces from one cage. One-way ANOVA with Dunnett's multiple comparisons. **b**, Plasma cytokines and chemokines of mice in Fig. 2. Mean ± s.d. Two-way ANOVA with Tukey's multiple comparisons. **c**, Representative spleen size of mice in Fig. 2. **d–f**, Total blood neutrophil count (**d**), platelet count (**e**) and spleen weight (**f**) from mice in Fig. 2, stratified by sex.

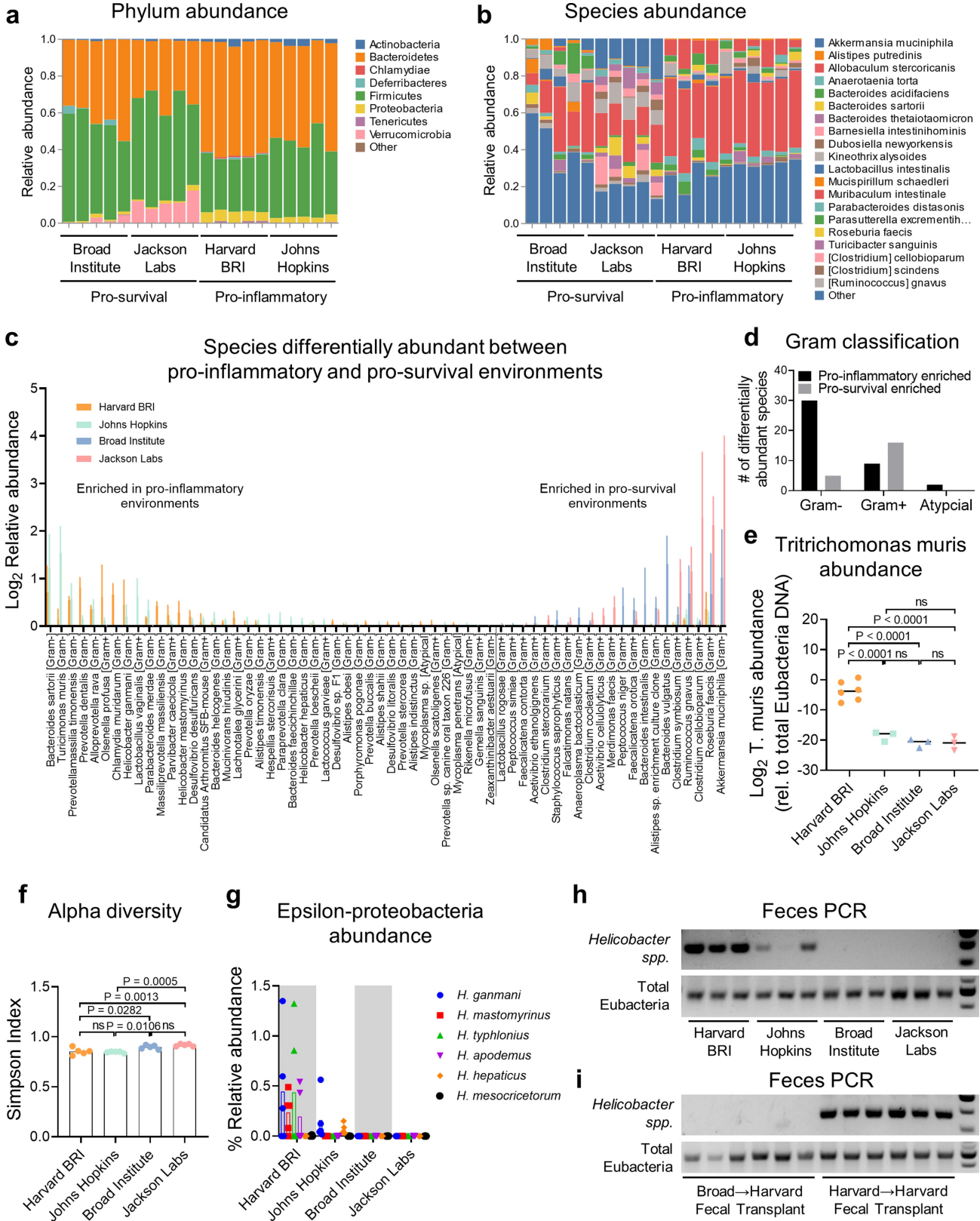
stratified by sex. **g, h**, Total blood neutrophil count (**g**) and platelet count (**h**) in 30-week-old C9orf72(Harvard) neo-deleted mice stratified by sex (C9orf72(Harvard)^{+/+}, n = 9 male and 13 female; C9orf72(Harvard)^{-/-}, n = 25 male and 27 female; C9orf72(Harvard)^{+/+}, n = 13 male and 9 female). **i**, Spleen weight in 40-week-old C9orf72(Harvard) neo-deleted mice stratified by sex (C9orf72(Harvard)^{+/+}, n = 8 male and 11 female; C9orf72(Harvard)^{-/-}, n = 13 male and 7 female; C9orf72(Harvard)^{+/+}, n = 12 male and 6 female). In **d–i**, each dot represents one mouse. One-way ANOVA with Sidak's multiple comparisons.

Article



Extended Data Fig. 4 | Acute antibiotic treatment improves motor function, and mitigates splenomegaly and cytokine burden, in C9orf72 LOF mice. **a**, Accelerating rotarod performance of mice in Fig. 3a. Each point represents the average of three trials per mouse. Two-way ANOVA with Dunnett's multiple comparisons. **b**, Plasma cytokines and chemokines of mice in Fig. 3a–d after seven weeks of treatment. **c, d**, Representative spleen size (**c**) and spleen weight (**d**) of mice in Fig. 3a after eight weeks of treatment. Each dot represents one mouse. One-way ANOVA with Sidak's multiple comparisons. **e**, Plasma cytokines and chemokines of mice in Fig. 3e–h 10 weeks after faecal transplant. In **b**, **e**, mean ± s.d. Two-way ANOVA with Tukey's multiple comparisons.

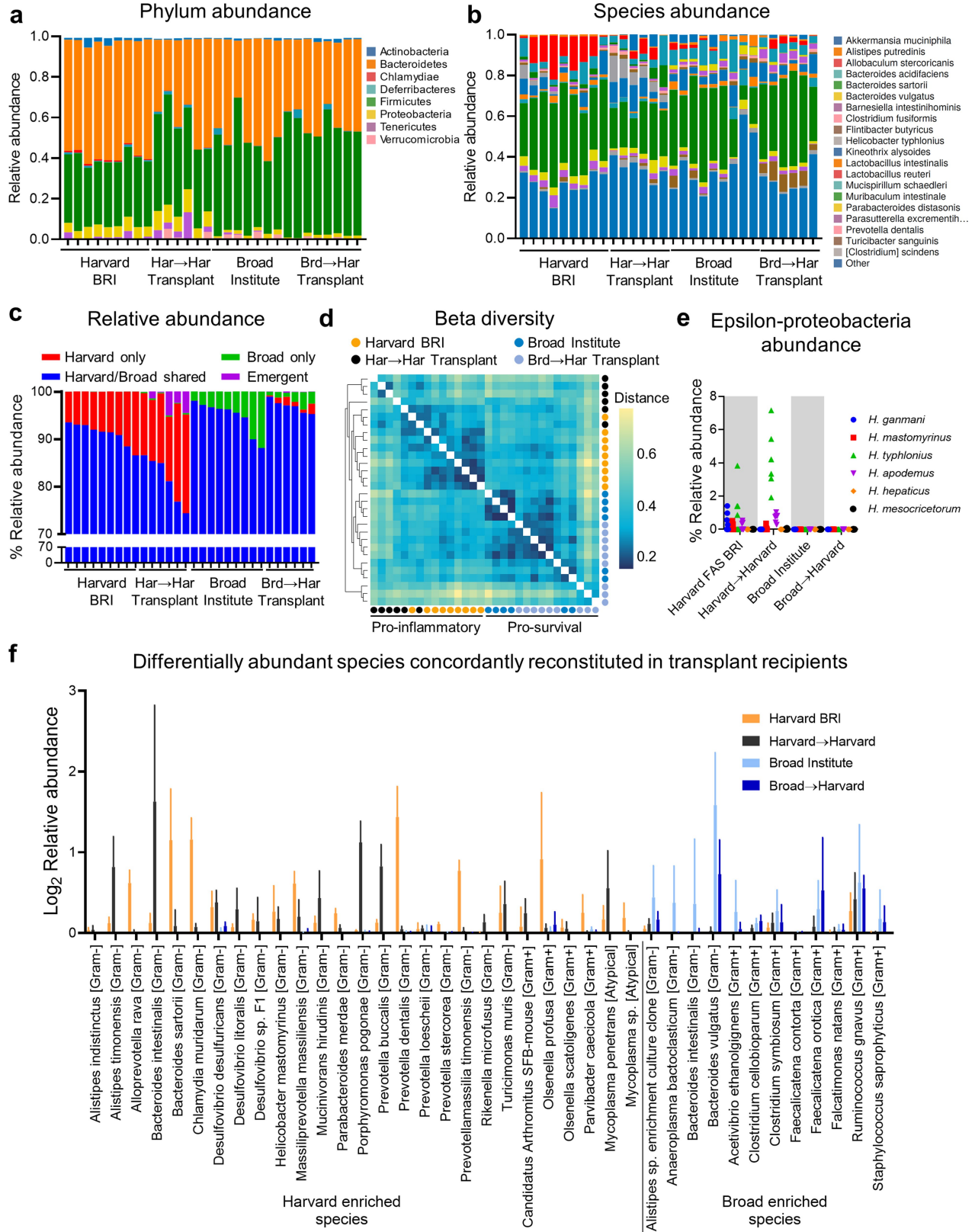
and spleen weight (**d**) of mice in Fig. 3a after eight weeks of treatment. Each dot represents one mouse. One-way ANOVA with Sidak's multiple comparisons. **e**, Plasma cytokines and chemokines of mice in Fig. 3e–h 10 weeks after faecal transplant. In **b**, **e**, mean ± s.d. Two-way ANOVA with Tukey's multiple comparisons.



Extended Data Fig. 5 | See next page for caption.

Article

Extended Data Fig. 5 | Bacteria and protozoa diversity across environments. **a, b**, Phylum-level (**a**) and species-level (**b**) relative abundance of bacteria from 16S rDNA sequencing in Fig. 3i. Each bar represents sequencing from one pellet per cage. **c, d**, Relative abundance (**c**) and Gram-stain classification (**d**) of bacterial species, the abundance of which was significantly different between pro-inflammatory environments (Harvard BRI and Johns Hopkins University) and pro-survival environments (Broad Institute and Jackson Laboratory). *t*-test with Bonferroni multiple comparisons; 62/301 detected species had significance $P < 0.0002$. $n = 5$ faecal pellets per environment. Mean \pm s.d. **e**, Quantitative PCR with reverse transcription analysis of *T. muris* 28S rDNA relative to total Eubacteria 16S rDNA in faeces. **f**, Simpson index of faecal α -diversity. **g**, Relative abundance of ϵ proteobacteria (*Helicobacter*). In **e–g**, each dot represents a faecal pellet from one cage. One-way ANOVA with Tukey's multiple comparisons. **h**, PCR analysis of *Helicobacter* spp. 16S rDNA and total Eubacteria 16S rDNA in faeces (six weeks after transplant) from Fig. 3e. **i**, PCR analysis of *Helicobacter* spp. 16S rDNA and total Eubacteria 16S rDNA in faeces (six weeks after transplant) from Fig. 3e.

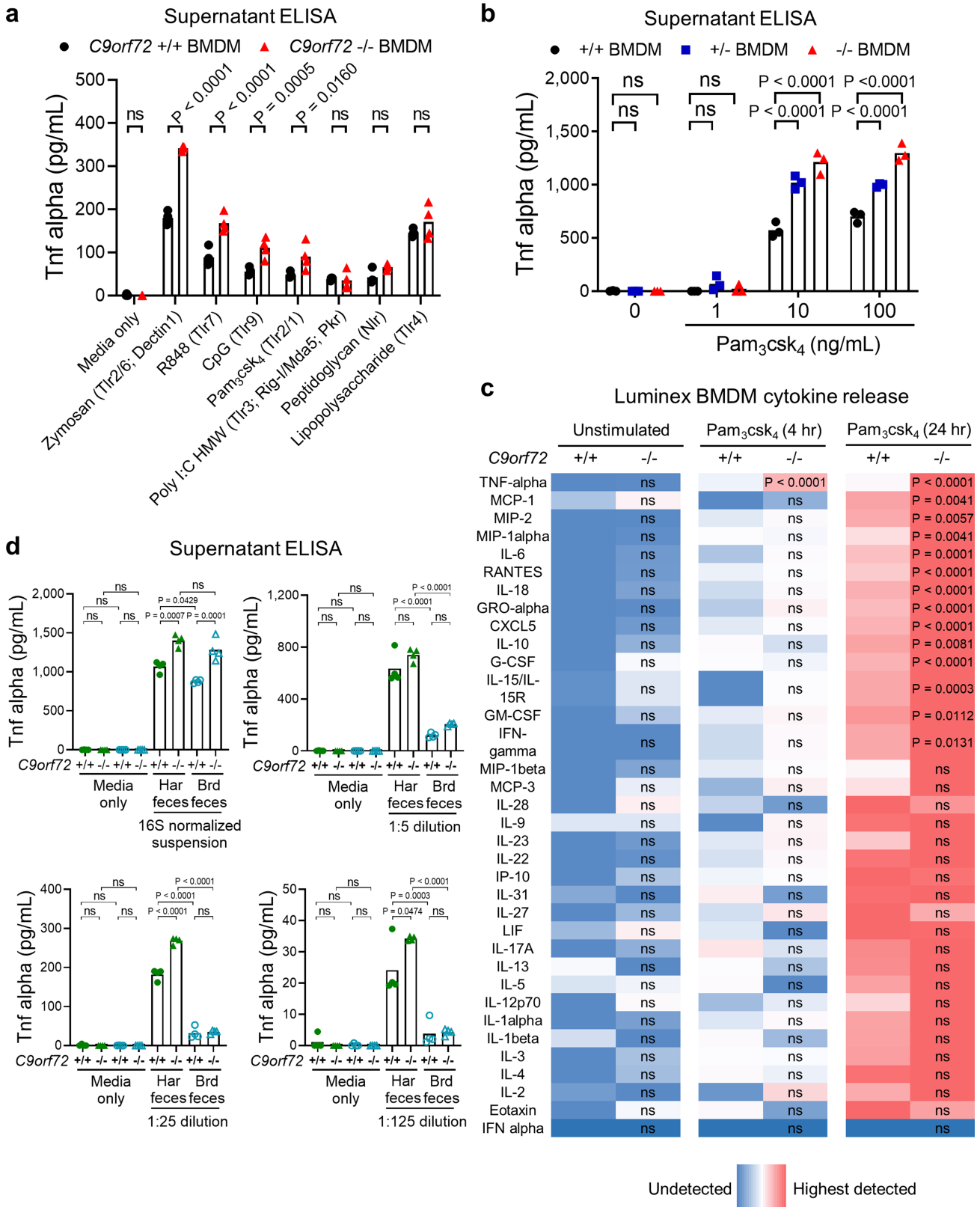


Extended Data Fig. 6 | See next page for caption.

Article

Extended Data Fig. 6 | Environment-enriched bacteria engraft faecal-transplant recipients. **a–f**, Analysis of bacteria in faeces at 10 weeks after transplant (from mice in Fig. 3e) by 16S rDNA sequencing. Each bar represents a faecal sample from an individual cage. **a, b**, Phylum-level (**a**) and species-level (**b**) relative abundance. **c**, Relative abundance of bacterial species grouped as those only observed in cages from Harvard BRI (Harvard-only), those only observed in cages from the Broad Institute (Broad-only), those observed in cages from Harvard BRI and the Broad Institute (Harvard/Broad-shared) or those not observed in Harvard BRI or Broad Institute cages

but detectable in transplant recipient cages (emergent). **d**, Bray–Curtis dissimilarity matrix of faeces β -diversity. **e**, Relative abundance of ϵ proteobacteria (*Helicobacter*). **f**, Putative pro-inflammatory species ($n=27$) enriched in pro-inflammatory environments (Harvard BRI and Johns Hopkins University) that were also enriched in Harvard-to-Harvard recipients, and putative pro-survival species ($n=12$) enriched in pro-survival environments (Broad Institute and Jackson Laboratory) and enriched in Broad-to-Harvard recipients.

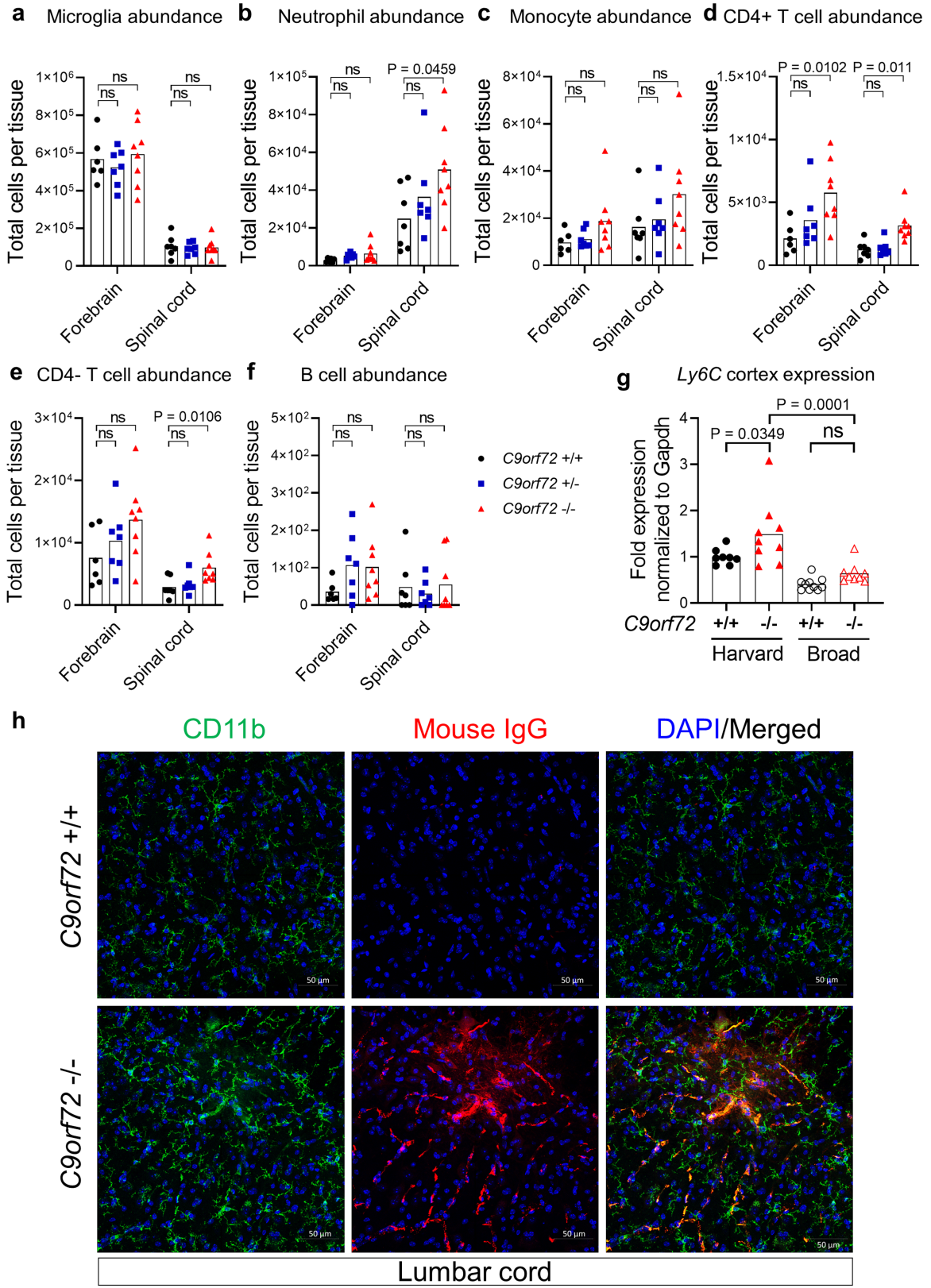


Extended Data Fig. 7 | See next page for caption.

Article

Extended Data Fig. 7 | *C9orf72* restricts myeloid cytokine release in response to foreign stimuli. **a–d**, Analysis of cytokines and chemokines in supernatant 24 h after stimulation of bone-marrow-derived macrophages (BMDM) with activators of Toll-like receptor (Tlr) or NOD-like receptor (Nlr) agonists (**a–c**) or filtered Eubacteria-normalized faecal preparations (**d**). **c**, The abundance of cytokine and chemokine in the supernatant was normalized and colour-coded (blue, low; red, high) relative to the average level of each molecule in unstimulated *C9orf72*^{+/+} bone-marrow-derived macrophage wells. Levels of each analyte were measured by Luminex in multiplex. **d**, The abundance of total Eubacteria in each faecal sample was measured by qPCR for

16S rDNA and this value was used to normalize faecal Eubacteria bacteria concentration before generation of the dilution curve. Each dot represents one well. Panels are representative of $n=2$ replicate experiments (**a**); $n=5$ replicate experiments (**b**); one representative experiment with average of $n=3$ technical replicates per condition (**c**); $n=2$ replicate experiments (**d**). In **a**, two-way ANOVA with Sidak's multiple comparison. In **b**, two-way ANOVA with Dunnett's multiple comparisons. In **c**, two-way ANOVA with Sidak's multiple comparison for each analyte tested. In **d**, one-way ANOVA with Sidak's multiple comparisons.

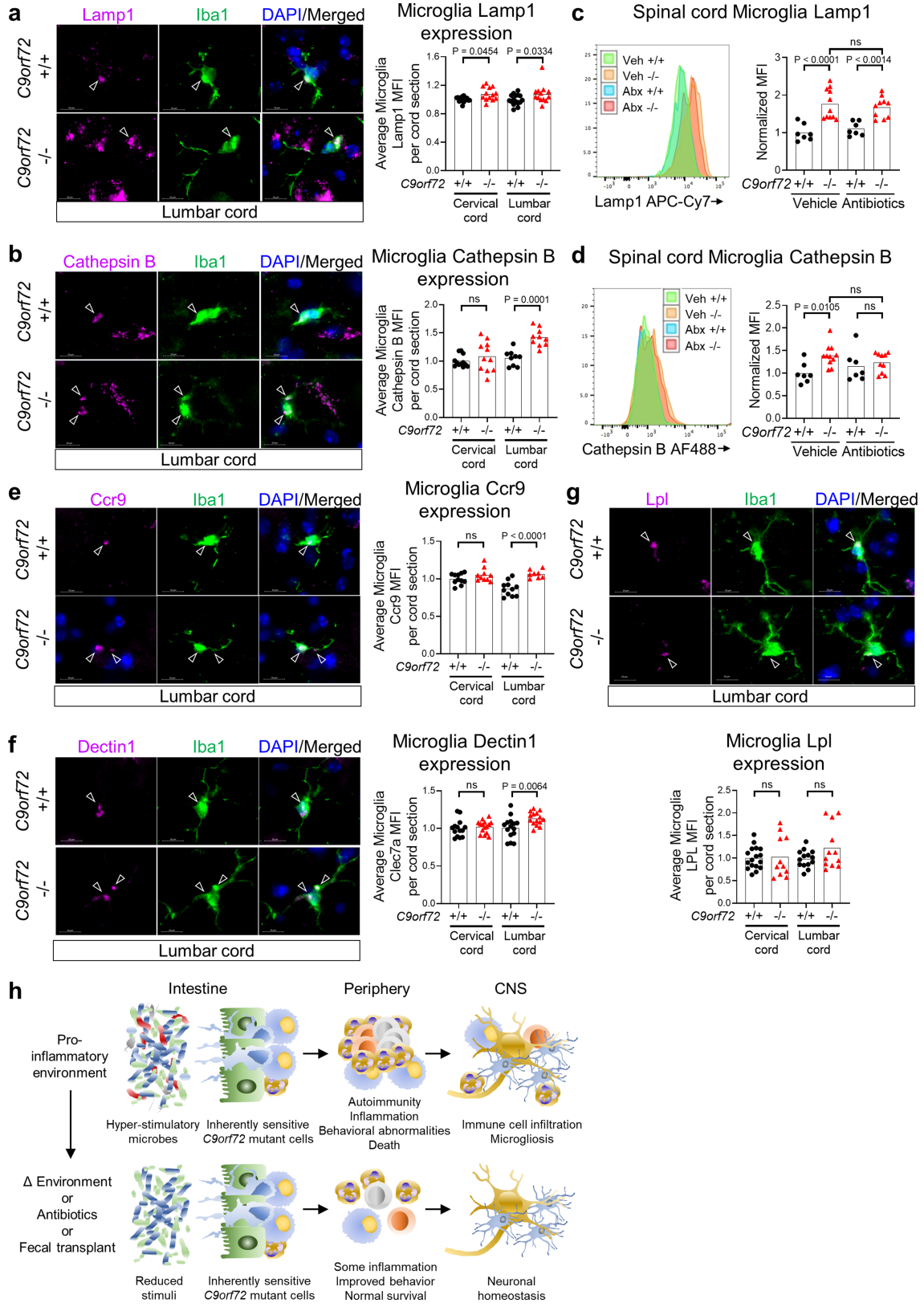


Extended Data Fig. 8 | See next page for caption.

Article

Extended Data Fig. 8 | Neutrophils and T cells infiltrate spinal cord of *C9orf72*LOF mice. **a–f**, Mass cytometry investigation of single-cell-dissociated forebrain or spinal cord from 36-week-old *C9orf72(Harvard)* neo-deleted male and female mice (*C9orf72(Harvard)*^{+/+}, $n=7$; *C9orf72(Harvard)*^{-/-}, $n=7$; *C9orf72(Harvard)*^{-/-}, $n=8$). One *C9orf72*^{+/+} forebrain sample failed, and was excluded from analysis. Representative gating scheme can be found in Supplementary Information. Populations were defined as CD45^{mid} CX3CRI⁺CD39⁺ microglia (**a**), CD45^{high}Ly6C⁺Ly6G^{high} neutrophils (**b**), CD45^{high}Ly6C⁺Ly6G^{low} monocytes (**c**), CD45^{high}CD3e⁺CD4⁺ T cells (**d**), CD45^{high}CD3e⁺CD4⁻ T cells (**e**) and CD45^{high}CD19⁺ B cells (**f**). Quantification of total cells per tissue was obtained by multiplying the percentage of each gated

population by the total cells recovered from the tissue of that mouse. Each dot represents one mouse. Two-way ANOVA with Dunnett's multiple comparisons. **g**, Quantitative PCR with reverse transcription of *Ly6c* expression in total cortex tissue of 47-week-old *C9orf72(Harvard)* neo-deleted mice (*C9orf72(Harvard)*^{+/+}, $n=8$; *C9orf72(Harvard)*^{-/-}, $n=9$) or *C9orf72(Broad)* neo-deleted mice (*C9orf72(Broad)*^{+/+}, $n=10$; *C9orf72(Broad)*^{-/-}, $n=9$). Each dot represents one mouse. One-way ANOVA with Sidak's multiple comparisons. **h**, Orthogonal projection of confocal imaging of CD11b and mouse immunoglobulin IgG in lumbar spinal cord of a 43-week-old *C9orf72(Harvard)* mouse.



Extended Data Fig. 9 | See next page for caption.

Article

Extended Data Fig. 9 | Elevated lysosomal proteins and microgliosis in spinal cords of *C9orf72*LOF mice. **a, b, e–g,** Orthogonal projection and quantification of confocal imaging of LAMP1 (**a**), cathepsin B (**b**), CCR9 (**e**), dectin 1 (CLEC7A) (**f**) and LPL (**g**) in IBA1⁺ microglia in spinal cord of a 55-week-old *C9orf72(Harvard)* mouse. One-way ANOVA with Sidak's multiple comparisons. Each dot represents the average mean fluorescent intensity (MFI) of the antigen within microglia on a given spinal cord section. Over 100 microglia were surveyed per section. Sections from $n=3$ *C9orf72*^{+/+} and $n=3$ *C9orf72*^{-/-} mice were surveyed. **c, d,** Flow cytometry quantification of

LAMP1 (**c**) or cathepsin B (**d**) in CD45^{mid}CD11b⁺CD39⁺ microglia from spinal cord of *C9orf72(Harvard)* neo-deleted mice in Fig. 2. One-way ANOVA with Sidak's multiple comparisons. **h,** Graphical illustration of *C9orf72* functioning within the haematopoietic system to restrict the development of inflammation, autoimmunity, peripheral immune infiltration into the central nervous system (CNS) and microgliosis in response to hyper-stimulatory communities of gut microflora. The microglia image was modified from Servier Medical Art (https://smart.servier.com/smart_image/microglia-2/) under a CC BY 3.0 licence.

Reporting Summary

Nature Research wishes to improve the reproducibility of the work that we publish. This form provides structure for consistency and transparency in reporting. For further information on Nature Research policies, see [Authors & Referees](#) and the [Editorial Policy Checklist](#).

Statistics

For all statistical analyses, confirm that the following items are present in the figure legend, table legend, main text, or Methods section.

n/a Confirmed

- The exact sample size (n) for each experimental group/condition, given as a discrete number and unit of measurement
- A statement on whether measurements were taken from distinct samples or whether the same sample was measured repeatedly
- The statistical test(s) used AND whether they are one- or two-sided
Only common tests should be described solely by name; describe more complex techniques in the Methods section.
- A description of all covariates tested
- A description of any assumptions or corrections, such as tests of normality and adjustment for multiple comparisons
- A full description of the statistical parameters including central tendency (e.g. means) or other basic estimates (e.g. regression coefficient) AND variation (e.g. standard deviation) or associated estimates of uncertainty (e.g. confidence intervals)
- For null hypothesis testing, the test statistic (e.g. F , t , r) with confidence intervals, effect sizes, degrees of freedom and P value noted
Give P values as exact values whenever suitable.
- For Bayesian analysis, information on the choice of priors and Markov chain Monte Carlo settings
- For hierarchical and complex designs, identification of the appropriate level for tests and full reporting of outcomes
- Estimates of effect sizes (e.g. Cohen's d , Pearson's r), indicating how they were calculated

Our web collection on [statistics for biologists](#) contains articles on many of the points above.

Software and code

Policy information about [availability of computer code](#)

Data collection

Flow cytometry and mass cytometry data was analyzed by Flowjo v10.6 or Cytobank Premium.

Data analysis

Image analysis was performed using ZEISS ZEN 2.6 image processing software. Videos were rendered using Bitplane Imaris 9.2. For 16S rDNA sequencing following the sequencing run, the sequence data was separated based on the nucleotide bar code and then compared to the Greengenes database. Relative abundance, alpha diversity, beta diversity and principal coordinate analysis was performed using QIIME analysis software (v2).

For manuscripts utilizing custom algorithms or software that are central to the research but not yet described in published literature, software must be made available to editors/reviewers. We strongly encourage code deposition in a community repository (e.g. GitHub). See the Nature Research [guidelines for submitting code & software](#) for further information.

Data

Policy information about [availability of data](#)

All manuscripts must include a [data availability statement](#). This statement should provide the following information, where applicable:

- Accession codes, unique identifiers, or web links for publicly available datasets
- A list of figures that have associated raw data
- A description of any restrictions on data availability

The 16S rDNA sequencing datasets generated and analyzed during the current study are available through the GEO repository at GSE147325. All other data generated or analyzed during this study are included in this published article (and its supplementary information files).

Field-specific reporting

Please select the one below that is the best fit for your research. If you are not sure, read the appropriate sections before making your selection.

Life sciences Behavioural & social sciences Ecological, evolutionary & environmental sciences

For a reference copy of the document with all sections, see nature.com/documents/nr-reporting-summary-flat.pdf

Life sciences study design

All studies must disclose on these points even when the disclosure is negative.

Sample size	Effect sizes of all phenotypic measures were estimated using GPower 3.1 software based on the average and standard deviation of each measure either from small trial experiments or previously published work on the model. These effect sizes were used to estimate necessary sample sizes for larger studies involving multiple treatment groups.
Data exclusions	Data were not excluded and values from each animal or replicate are indicated on the graphs as stated in figure legends
Replication	All attempts at replication were successful. To ensure reproducibility, independent cohorts of animals were repeatedly generated and tested for the presence of phenotypes described. In the case where survival differed when mice were reared in different environments, mechanistic experiments were performed to understand what environmental factors contributed to differences observed.
Randomization	In Figures 1, 2 and 4, age matched animals born from heterozygous inter-crosses were assigned to each cohort for study. In Figure 3, mutant animals were pre-screened for behavioral performance, neutrophilia and psuedothrombocytopenia and animals demonstrating these phenotypes were licensed into the trial as described in the manuscript text.
Blinding	Researchers performing behavioral tasks, bleeding animals, and administering antibiotics or vehicle treatment or feces were blinded to genotype.

Reporting for specific materials, systems and methods

We require information from authors about some types of materials, experimental systems and methods used in many studies. Here, indicate whether each material, system or method listed is relevant to your study. If you are not sure if a list item applies to your research, read the appropriate section before selecting a response.

Materials & experimental systems

n/a	Involved in the study
<input type="checkbox"/>	<input checked="" type="checkbox"/> Antibodies
<input checked="" type="checkbox"/>	<input type="checkbox"/> Eukaryotic cell lines
<input checked="" type="checkbox"/>	<input type="checkbox"/> Palaeontology
<input type="checkbox"/>	<input checked="" type="checkbox"/> Animals and other organisms
<input checked="" type="checkbox"/>	<input type="checkbox"/> Human research participants
<input type="checkbox"/>	<input type="checkbox"/> Clinical data

Methods

n/a	Involved in the study
<input type="checkbox"/>	<input checked="" type="checkbox"/> ChIP-seq
<input type="checkbox"/>	<input checked="" type="checkbox"/> Flow cytometry
<input checked="" type="checkbox"/>	<input type="checkbox"/> MRI-based neuroimaging

Antibodies

Antibodies used

Immunofluorescence: Rat-anti-mouse/human CD11b-FITC 1:200 (M1/70, BioLegend 101205), rabbit-anti-mouse/human Cathepsin B 1:400 (D1C7Y CST, 31718S), rat-anti-mouse Ly6C-647 1:1000 (HK1.4 BioLegend, 128009), rat-anti-mouse CD45-488 1:200 (30-F11 BioLegend, 103121), guinea pig-anti-mouse Iba1 1:500 (234004 Synaptic Systems), rat-anti-mouse/human Lamp1 1:200 (1D4B SCB, sc-19992), rat-anti-mouse Dectin1/Clec7a 1:30 (Invivogen, mabg-mdect), mouse-anti-mouse-Lpl LPL.A4 1:200 (Abcam, ab21356). Donkey-anti-rat-AlexaFluor-488 (Invitrogen, A-21208), Donkey-anti-mouse IgG-555 (Invitrogen, A-31570), Goat-anti-rabbit-555 (Invitrogen, A-21428), Goat-anti-rabbit-647 (Invitrogen, A27040), Goat-anti-rat-647 (Invitrogen, A-21247), Goat-anti-guinea pig-647 (Invitrogen, A-21450), all 1:500 dilution.
 Flow cytometry: (BioLegend): rat-anti-mouse CD45-BV421 (103103) or APC-Cy7 (103115) 1:200 (30-F11), rabbit-anti-mouse/human Cathepsin B 1:100 FACS (D1C7Y CST, 31718S) and donkey anti-rabbit-AlexaFluor-488 1:500 (Invitrogen, A-21206), rat-anti-mouse-Ccr9-FITC 1:200 (9B1, Biolegend, 129705), rat-anti-mouse F4/80-PE-Cy5 1:400 (BM8, Biolegend, 123111), rat-anti-mouse/human CD11b-AlexaFluor-700 1:400 (M1/70, Invitrogen, 56-0112-82), rat-anti-mouse Lamp1-APC-Cy7 1:400 (1D4B, Biolegend, 121615), TruStain FCX rat-anti-mouse CD16/32 1:250 (93, Biolegend, 101319), rat-anti-mouse CD39-PE 1:400 (Duoh59, Biolegend, 143803), rat-anti-mouse Ly6G-PE-Cy7 1:600 (1A8, Biolegend, 127617), rat-anti-mouse Ly6C-AlexaFluor-647 (HK1.4, Biolegend, 128009).
 Mass cytometry: (All Fluidigm 1:150) Rat-anti-mouse Ly6G-141Pr 1A8 (3141008B), Rat-anti-mouse CD39-142Nd 24DMS1 (3142005B), rat-anti-mouse CD4-145Nd RM4-5 (3145002B), Rat-anti-mouse CD45-147Sm 30-F11 (3147003B), Rat-anti-mouse/human CD11b-148Nd M1/70 (3148003B), Rat-anti-mouse CD3e-152Sm 145-2C11 (3152004B), Rat-anti-mouse CD19-166Er 6D5 (3166015B), rat-anti-mouse CX3CR1-164Dy SA011F11 (3164023B). Rat-anti-mouse Ly6C-143Nd HK1.4 1:150 (Biolegend, 128039).

Validation

Description of antibody validations are provided by each commercial manufacturer on their associated website. Each lot of Biolegend antibodies were quality control tested by immunofluorescent staining with flow cytometric analysis. The Cell Signaling Technology Cathepsin B (D1C7Y) XP antibody met all of the quality control standards and was approved for Flow Cytometry, Immunofluorescence, Immunohistochemistry and Western. The SCB Lamp1 1D4B antibody was recommended for detection of LAMP1 of mouse, rat and human origin by WB, IP, IF and FCM. The Synaptic Systems guinea pig anti-mouse Iba1 was approved for WB, IP, ICC, and IHC and reacts with mouse, human, rat, sheep and ape with no signal in zebrafish. The Invivogen rat anti-mouse Dectin1 mabg-mdect antibody was screened for flow cytometry and neutralization activity and recognizes both mDectin-1 isoforms A and B. The Abcam mouse anti-mouse-Lpl LPLA4 antibody was suitable for ICC/IF, IHC-P, Flow Cyt, WB and ELISA with reactivity against mouse, human and cow. The Invitrogen CD11b-AF700 M1/70 antibody was published to react with mouse, human and fish. For Invitrogen secondary antibodies, they show minimum cross-reactivity to species other than the intended target and are approved for Flow, ICC, IF and WB. Fluidigm 600 Maxpar metal conjugated antibodies were predesigned for mass cytometry. Each antibody was validated empirically by performing dilution series on tissue or cells expressing the relevant antigens in relation to isotype or buffer controls

Animals and other organisms

Policy information about [studies involving animals; ARRIVE guidelines](#) recommended for reporting animal research

Laboratory animals

C9orf72 loss of function neo deleted animals were previously generated using the Knockout Mouse Project targeting vector on C57BL6/J background and crossed with mice expressing Sox2-cre to remove the neomycin resistance cassette. Male and Female mice were studied in Figure 1 (Harvard BRI C9orf72 +/+ n=12; +/- n=13; -/- n=10 with mean age 47.7 weeks s.d. 2.3 weeks; Broad Institute C9orf72 +/+ n=12; +/- n=18; -/- n=11 with mean age 47.9 weeks s.d. 3.2 weeks) and Figure 2 (vehicle +/+ n=7; -/- n=11 mean age 3.3 weeks s.d. 0.8 weeks or antibiotics +/+ n=7; -/- n=11 mean age 3.4 weeks s.d. 1.2 weeks) while only female mice were studied in Figure 3a (vehicle +/+ n=12; -/- n=12 mean age 35.3 s.d. 1.9 weeks or antibiotics +/+ n=13; -/- n=12 mean age 35.8 weeks s.d. 1.4 weeks) and 3e (Harvard BRI feces +/+ n=13; -/- n=17 mean age 13.3 weeks s.d. 3.8 weeks or Broad Institute feces +/+ n=14; -/- n=15 mean age 13.3 weeks s.d. 3.8 weeks). For confocal imaging in Figure 4 n=3 +/+ and n=3 -/- male 55 week old mice used.

Wild animals

The study did not involve wild animals.

Field-collected samples

The study did not involve samples collected from the field.

Ethics oversight

All experimental procedures were approved by the Institutional Animal Care and Use Committee of Harvard University and the Broad Institute.

Note that full information on the approval of the study protocol must also be provided in the manuscript.

Flow Cytometry

Plots

Confirm that:

- The axis labels state the marker and fluorochrome used (e.g. CD4-FITC).
- The axis scales are clearly visible. Include numbers along axes only for bottom left plot of group (a 'group' is an analysis of identical markers).
- All plots are contour plots with outliers or pseudocolor plots.
- A numerical value for number of cells or percentage (with statistics) is provided.

Methodology

Sample preparation

Animals were anesthetized with isoflurane followed by transcardial perfusion with HBSS supplemented with 10 U/mL heparin. Spleens were dissociated by repeated trituration with glass pipettman in HBSS, subjected to 10-minute RBC lysis (eBioscience), washed in autoMACS (Miltenyi), filtered (40 µm) and counted using Countess (Invitrogen) for antibody staining. For flow cytometry of the CNS, spinal cords were digested by papain and DNase diluted in EBSS (Worthington) for 10 minutes at 37°C, triturated with glass pipettman to generate large tissue chunks then allowed to digest for 20 minutes at 37°C. DMEM supplemented with glutamax was added, samples triturated to single cells, ovomucoid (Worthington) and DNase diluted in EBSS added to inhibit protease activity, cells filtered, washed in autoMACS buffer, and pelleted at 500xg for 15 minutes at 4°C. Cell pellets brought up in isotonic Percoll Plus (Sigma) diluted to 30% in autoMACS and spun for 15 minutes at room temperature with no brake. Floating myelin was gently removed using plastic transfer pipette. Cell pellets were resuspended, filtered, washed in autoMACS and re-pelleted at 4°C. Cells were fixed in 4% paraformaldehyde (PFA; Electron Microscopy Sciences) either before or after antibody staining depending on need.

Instrument

Samples collected on BD LSRII

Software

Flow cytometry and mass cytometry data was analyzed by Flowjo v10.6 or Cytobank Premium.

Cell population abundance

No experiments involving cell sorting are described

Gating strategy

Cells were defined based on Fsc-A and Ssc-A profile, then single cells were gated based on horizontal ratio of Fsc-A/Fsc-W and then Ssc-A/Ssc-W. CD45+ cells were sub-gated based on CD45/Ssc-A using samples without anti-CD45 antibody to define the

negative population. From the CD45+ gate, CD45/CD11b was used to define CD45mid CD11b+ microglia and CD45hi CD11b+ infiltrating myeloid cells. From the CD45+ gate, CD45mid CD11b+ microglia were confirmed to be CD39+, while CD45hi CD11b+ infiltrating myeloid cells were confirmed to be Ly6C+.

Tick this box to confirm that a figure exemplifying the gating strategy is provided in the Supplementary Information.